3 Chitosan-g-estrone nanoparticles of palbociclib for hypoxic breast tumor therapy

3.1 Objective of the study

- The objective of this study is to develop palbociclib loaded ER targeted chitosan nanoparticles for the targeted delivery to hypoxic breast tumors.
- To characterize their physicochemical properties, *in vitro* characterization, and *in vivo* evaluation.
- To conduct *in vivo* pharmacokinetic study, anticancer efficacy, optical, ultrasound/photoacoustic imaging and survival study.

3.2 Plan of study

- Preparation of PLB loaded ER targeted chitosan NPs using solvent evaporation combined with ionic cross-linking method
- Physicochemical and in-vitro evaluation of dual receptor targeted NPs
- Particle size, polydispersity index, and zeta potential by DLS
- Electron microscopy (SEM, TEM & AFM)
- Crystallographic studies by XRD
- Surface chemistry by XPS
- Determination of entrapment efficiency
- *In vitro* drug release studies
- *In vitro* cellular uptake study on MCF-7 and T-47D cells
- *In vitro* cytotoxicity study on MCF-7 and T-47D cells
- *In vitro* cell cycle study on MCF-7 cells
- *In vivo* pharmacokinetic and histopathology studies in SD rats
- Optical, ultrasound/photoacoustic imaging of the rat breast tumor
- Anticancer efficacy studies on DMBA induced breast tumor rat model, tumor targeting efficiency and survival analysis.

3.3 Materials

Palbociclib was provided by Sun Pharmaceutical Industries Ltd. (Gurugram, India) as a gift sample. Chitosan (CS) (molecular weight ~1.5 kDa, degree of deacetylation ≥90%), estrone (Egen), succinic anhydride (SA), Na-tripolyphosphate, 4-dimethylaminopyridine (DMAP), N-hydroxysuccinimide (NHS), triethylamine (TEA), and N-(3-dimethylaminopropyl)-N-ethylcarbodiimide (EDC) were supplied by Sisco Research Laboratories Pvt. Ltd. (SRL, India). The human breast cell lines MCF-7 and T-47D were procured from NCCS Pune, India. Dulbecco's modified Eagle medium (DMEM), fetal bovine serum (FBS), trypsin−EDTA, penicillin−streptomycin solutions, and 12-well cell culture plates were purchased from Cell Clone (Genetix Biotech Asia Pvt. Ltd.). The T-25 cell culture flask and 96-well plates were obtained from Eppendorf. 1,1′-Dioctadecyl-3,3,3′,3′-tetramethylindodicarbocyanine, 4-chlorobenzene sulfonate salt (DiD dye) was purchased from Thermo Fisher Scientific, India. The remaining chemicals used in the experiment were of analytical grade.

3.4 Methods

3.4.1 Synthesis of chitosan-g-estrone (CS-g-Egen) conjugate

3.4.1.1 Activation of Egen-COOH

The carboxylic acid group was functionalized to Egen, by a ring opening polymerization reaction in the presence of SA and DMAP [101]. Egen (1000 mg, 3.7 mmol), TEA (112 mg, 11.12 mmol), and DMAP (46 mg, 0.37 mmol) were solubilized in dry THF (8 mL) under magnetic stirring in a roundbottom flask, and then SA (740 mg, 7.4 mmol) was added to the above mixture and stirred until completely dissolved. The above reaction mixture was agitated for 42 h at 25 ± 2 °C, and then samples were further concentrated by vacuum centrifugation and dissolved in 10 mL of distilled water. The pH of the resultant solution was adjusted to pH 9−10 by using K_2CO_3. The above reaction mixture was filtered to remove the unreacted reactants. Further, the filtrate was adjusted to

pH 1−2 with dil. HCl. The formed precipitate was separated and dried to get Egen-COOH (1265.5 mg, 92% yield) [49].

3.4.1.2 Conjugation of CS with activated Egen-COOH

Carbodimide chemistry was used for the preparation of the Egen-COOH conjugated CS (CS-g-Egen) graft polymer. The conjugation reaction was mediated by NHS/EDC. The mixture of Egen-COOH (160 mg, 0.6 mmol), NHS (69 mg, 0.6 mmol), and EDC (115 mg, 0.6 mmol) was transferred into anhydrous dichloromethane (DCM) and stirred by a magnetic stirrer (REMI 1 MLH) at room temperature. Following the evaporation of DCM, the residue was transferred to the solution of CS in 1% v/v glacial acetic acid at pH 4. The reaction was finished after 24 h, and the graft polymer was lyophilized (Labocon 4.5 L, United Kingdom) after being dialyzed for 72 h against distilled water to eliminate any remaining free reactants [102].

3.4.1.3 Characterization of CS-g-Egen conjugate

CS, Egen, Egen-COOH, and CS-g-Egen were characterized by FTIR, NMR and mass spectroscopy for their identification and confirmation of Egen-COOH and CS-g-Egen synthesis.

3.4.1.4 Degree of Egen substitution

The degree of Egen substitution on CS was estimated with the help of a multimode microplate reader (Molecular Devices, USA). Preferentially, the CS-g-Egen (4 mg) sample was sonicated in a water bath sonicator for 4 h in a solution of DMSO/DCM (8:2). The vortexed samples were subjected to centrifugation (REMI Cooling Centrifuge) for 30 min at 10,000 rpm and then filtered and analyzed in the UV mode of the microplate reader. The concentration of Egen in the sample was estimated by using a standard calibration curve of Egen plotted at λmax of 296 nm [103, 104]. The following formula was used for the calculation:

$$Degree\ of\ Egen\ substitution = \frac{Egen/MWEgen}{(CSEgen - Egen)/MWCS}$$

Where, Egen indicates the concentration of estrone in the sample, MWEgen is the molecular weight of the Egen, CSEgen represents amount of the CS-g-Egen used in this experiment, and molecular weight of the CS has been indicated by MWCS.

3.4.2 Preparation of NPs

The PLB loaded nontargeted nanoparticles (PLB-CS NPs) and targeted nanoparticles (PLB-CS-g-Egen NPs) were formulated by modified solvent evaporation with an ionic crosslinking method [103]. Briefly, 30 mg of the CS was dissolved in 4 mL of the 0.2% v/v glacial acetic acid solution, and the pH of the mixture solution was raised to pH 5.5 with the help of NaOH. Further, 20 mg of the TPGS was dissolved in the above solution. Concisely, 1 mL of chloroform containing 3 mg of PLB was transferred to the above CS solution under ultrasonication, and an emulsion was made by utilizing an ultrasonic homogenizer (Hielscher UP200H, Germany). The ultrasonic homogenizer was set at an amplitude of 60%, and emulsification was performed for 3 min. The formed emulsion was subjected to magnetic stirring for 4 h to complete the evaporation of the chloroform, and then 1 mL of the solution of sodium tripolyphosphate (sod. TPP, 1 mg/mL) was added dropwise to the NP suspension for the cross-linking under magnetic stirring. The larger NPs were removed by centrifugation at 3000 rpm for 5 min. Further, the NP suspension was subjected to centrifugation at 10,000 rpm for 15 min, the transparent supernatant was discarded, and the NP pellets were washed with distilled water. The pellets were redispersed in 10 mL of normal saline (pH 7.4).

Targeted NPs were prepared in a similar manner by replacing 10 mg of CS with 10 mg of CS-g-Egen. Similarly, CM6 loaded NPs of all CS NPs were prepared by replacing PLB with 0.3 mg of CM6 for the cellular uptake study. Further, 2 µg DiD was used instead of PLB for the preparation of the DiD-CS NPs and DiD-CS-g-Egen NPs by a similar

process for the *in vivo* fluorescence imaging study in the rats. The composition of the various NPs formulations is presented in **Table 3.1**. The general method of chitosan NPs preparation is presented in **figure 3.1**.

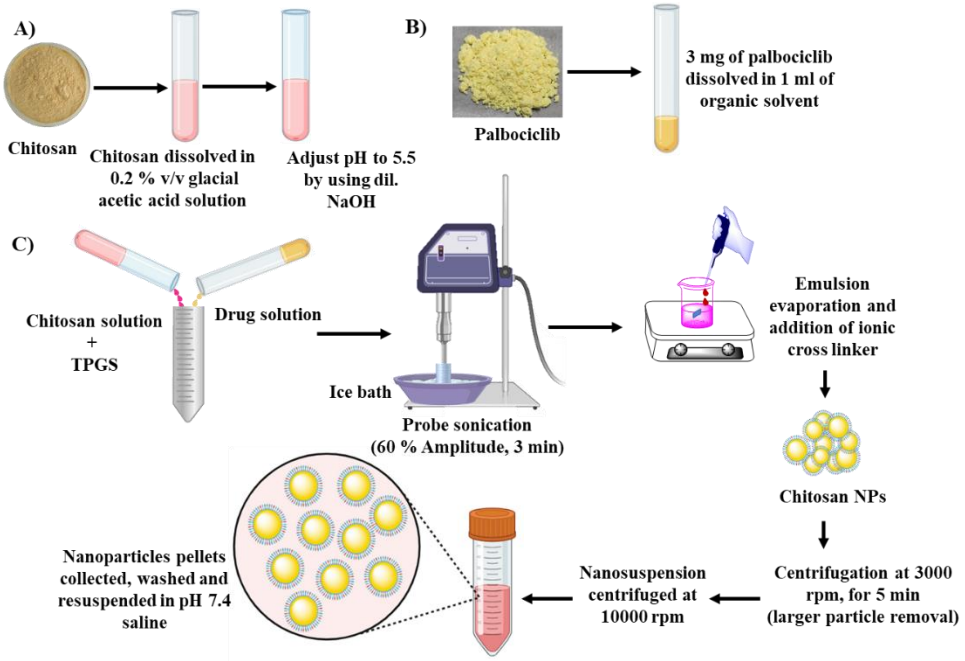

Figure 3.1. Method of preparation of chitosan NPs by solvent evaporation/ionic crosslinking

Table 3.1 Composition of the various NPs formulations

Batches	CS (mg)	TPGS (mg)	CS-g-Egen (mg)	Palbociclib (mg)	CM6 (mg)	Sod. TPP (mg)
Blank CS NPs	30	20	-	-	-	1
PLB-CS NPs	30	20	-	3	-	1
PLB-CS-g-Egen NPs	20	20	10	3	-	1
CM6-CS NPs	30	20	-	-	0.3	1
CM6-CS-g-Egen NPs	20	20	10	-	0.3	1

Blank CS NPs: Blank chitosan nanoparticles
PLB-CS NPs: Non-targeted PLB loaded chitosan nanoparticles
PLB-CS-g-Egen NPs: Estrogen receptor targeted PLB loaded chitosan nanoparticles
CM6-CS NPs: Non-targeted coumarin-6 loaded chitosan nanoparticles
CM6-CS-g-Egen NPs: Estrogen receptor targeted coumarin-6 loaded chitosan nanoparticles

3.4.3 Characterization of nanoparticles

3.4.3.1 Particle size, zeta potential and polydispersity index

The prepared NPs were evaluated for their mean particle size and zeta potential by using Zetasizer (Nano ZS90, Malvern Instruments). Particle size analysis was based on

dynamic light scattering (DLS) and zeta potential was analyzed on the basis of the electrophoretic mobility of the particles under electric fields [105].

3.4.3.2 Entrapment efficiency and drug loading capacity

The percentage of the entrapped drug inside the NPs were estimated by using a validated RP-HPLC (Simadzu LC-20AR, Japan) analytical method [106]. Briefly, 0.2 ml of the NP suspension was evaporated in the rotary evaporator and the residue was dispersed in the 1 ml of the methanol and sonicated in a water bath sonicator for 1 hr to break the NPs. The samples were centrifuged at 10000 rpm for 15 min and, filtered through a 0.22 µm nylon filter and analyzed by HPLC after suitable dilution in the mobile phase. The standard calibration curve of the PLB was linear in the range of 10-60 ng/ml (R^2= 0.9994). The HPLC method was used for the PLB analysis consisting of mobile phase A: acetonitrile and mobile phase B: methanol in the ratio of 30:70. The chromatographic conditions for the RP-HPLC analysis were 1 mL/min flow rate, 100 µL injection volume, 4.8 min retention time, and a photodiode array detector (λ_{max} = 355). A Shimadzu Shim-pack C18 column was used in the HPLC.

The percentage entrapment of the CM6 in the NPs were calculated by using the fluorescence mode of the microplate reader. After the sample preparation, reading was taken in the fluorescence mode with excitation at 462 nm and emission at 502 nm in chloroform and a standard curve was linear (10-100 ng/ml) with R^2 = 0.999.

The entrapment efficiency (EE) was estimated by using the following equations:

$$Entrapment\ efficiency\ (\%) = \frac{Amount\ of\ the\ drug\ entrapped\ in\ the\ NPs}{Amoun\ of\ the\ drug\ used\ in\ the\ NPs\ preparation} * 100$$

3.4.3.3 High resolution scanning electron microscopy (HR-SEM)

At room temperature, the morphologies of the developed PLB-CS NPs and PLB-CS-g-Egen NPs were captured by using a high-resolution electron microscope (Nova Nano SEM 450, FEI USA). The HR-SEM was set at 15 kV with a magnification of 200 KX. The

PLB-CS NP and PLB-CS-g-Egen NP suspensions were further diluted 10 times with distilled water, and a drop of the sample was cast on a separate glass slide, evenly spread, and dried for 12 h in a vacuum dryer. The prepared samples were coated with carbon, and microscopic images were captured [107].

3.4.3.4 High resolution transmission electron microscopy (HR-TEM)

PLB-CS NPs and PLB-CS-g-Egen NPs images were captured by using HR-TEM (Tecnai G2 20 TWIN, FEI USA). The NPs samples were diluted 10 folds with distilled water and cast on a separate carbon coated copper TEM grid with a 400 mesh size. The NPs casted TEM grid was vacuum dried, and microscopic images were captured at a voltage of 100 KV [108].

3.4.3.5 Atomic force microscopy (AFM)

Additionally, two dimensional (2D) and three dimensional (3D) images of the NPs were captured by using AFM (NTEGRA Prima, Netherlands). A drop of NPs suspension, after 10 times dilution with distilled water, was cast on the individual glass slide and homogenously distributed to form a thin film. Further, samples cast as a film were dried in the vacuum drier under reduced pressure. The images were captured and processed by using AFM image analysis software (Nova Px, NT-MDT Netherlands) [109].

3.4.3.6 Surface chemistry

Surface chemistry analysis of the PLB-CS NPs and PLB-CS-g-Egen NPs was done by utilizing X-ray photoelectron spectroscopy (XPS; Thermo Scientific K-Alpha XPS System) to confirm the NPs surface elemental composition in fixed transmission mode with binding energies in the range of 0–800 eV. Similarly, sample preparation for the XPS involves the casting of a suitably diluted NPs suspension in distilled water on a glass slide and after drying in the vacuum oven under reduced pressure, samples were analysed [110].

3.4.3.7 Egen surface content

The content of the Egen in PLB-CS-g-Egen NPs was calculated by a multi-mode microplate reader (Molecular Devices, USA). In brief, 0.2 ml of the NPs was lyophilized and transferred into a mixture of DMSO: DCM (4:1). The sample was subjected to vortexing for 4 h, and centrifuged. The supernatant was collected and passed through the 0.22 µm filter, and filtrate was analyzed in UV-Vis mode of the microplate reader at a fixed λ max = 296 nm [111]. The sample was compared with the standard calibration curve of the Egen. The total Egen content in the PLB-CS-g-Egen NPs was determined by the given formula.

$$Egen\ surface\ content\ (\%) = \frac{Egen\ content\ determined\ in\ the\ nanoparticles}{Total\ Egen\ content\ unsed\ in\ the\ nanoparticles} * 100$$

3.4.3.8 X-ray diffraction study

X-ray diffraction (XRD) is the characterization technique used to observe any crystalline peaks in the excipients, drugs, and their formulations. The physical state of the drug in the formulation can be determined by using the Rigaku MiniFlex X-ray diffractometer. A voltage of 40 kV and a current of 15 mA were applied to the samples, 5-50° was the sample scanning range (2θ), and the scan speed was 7°/min [112].

3.4.4 *In vitro* studies

3.4.4.1 *In vitro* drug release

The *in vitro* drug release of the PLB from the NPs was evaluated in phosphate buffer saline (PBS pH 7.4) and acetate buffer (pH 5.5). The principle of dialysis bag diffusion was applied for the understanding of the PLB release behavior from the NPs. The volume of the NPs equivalent to 0.3 mg PLB was transferred to a dialysis bag (1 kDa, MWCO), sealed hermetically, and immersed into 100 mL of the release medium. The system was maintained at 37 ± 5 °C with continuous shaking at 100 rpm. An equal volume of the fresh release medium was replaced after each predetermined sampling time point from the

receptor compartment. The collected samples were appropriately diluted and filtered through a 0.22 µm PVDF filter before being collected into the HPLC vials. *In vitro* release of the PLB was calculated by HPLC; the analytical method was similar to that used for the calculation of entrapment efficiency [102].

3.4.4.2 Hemolysis and hemocompatibility study

The compatibility of the developed formulation with the human blood was evaluated to understand the effect of the NPs on red blood cells. A sample of the 5 ml blood was collected from the blood bank in a tube containing EDTA and RBCs and separated by centrifugation at 2000 rpm. The formed pellets of the RBCs at the bottom of the centrifuge tube were washed 2-3 times with normal saline and suspended in normal saline. Further, 900 µl of RBCs suspension was incubated with 100 µl of various formulations (i.e., PLB, PLB-CS NPs, and PLB-CS-g-Egen NPs). For positive control, RBCs were suspended in distilled water, whereas negative control or blank RBCs were suspended in normal saline. These samples were incubated at 37°C for 1 h under gentle shaking. The distilled water causes 100 % hemolysis due to the permeation of the water to the RBCs and, causing it to swell and burst. After incubation, a drop of the samples was cast on the separate glass slides, and the smear was prepared and stained with Leishman stain. After completion of the staining procedure, images of the stained RBCs were captured by using a bright microscope. Further, incubated samples were centrifuged for 5 min at 2000 rpm. The supernatant of the samples was collected, and absorbance was measured at 540 nm using a multimode microplate reader (UV-Vis mode). As per the ASTM E2524-22 testing method for the hemolysis of the NPs. The negative control should be not more than 2%, and if the hemolysis % of the test materials is more than 5 %, it indicates that they may cause hemolysis if administered intravenously [113].

$$\% \, Hemolysis = \frac{Abs\ Test - Abs\ negative\ control}{Abs\ Positive\ control - Abs\ negative\ control} * 100$$

3.4.4.3 Cell culture and cell line maintenance

Mammalian breast cancer cell lines T-47D and MCF-7 were cultured in Dulbecco's modified eagle medium (DMEM) containing 10 % fetal bovine serum (FBS) along with Penicillin-Streptomycin antibiotic solutions. The cells were grown in a humidified CO_2 incubator, and 5 % of the CO2 was supplied throughout the experiment.

3.4.4.4 Cellular uptake study

The cellular uptake of free CM6, CM6-CS NPs and CM6-CS-g-Egen NPs was studied in the MCF-7 cell line by confocal microscopy (super resolution confocal microscopy, Leica, Germany). In brief, 1×10^5 MCF-7 cells were grown for 24 h on a cover slip in 6 well cell culture plate. Then, cells were incubated with each of the free CM6, CM6-CS NPs and CM6-CS-g-Egen NPs at 5 µg/ml concentration for 2 h. Then, cells were washed two times with the cold PBS. After incubation, the cells were fixed by using 4 % paraformaldehyde. Further cells were again washed three times with cold PBS. Fixed cell nuclei were stained by incubation with propidium iodide (PI) for another 30 min. Targeting efficiencies of the NPs were evaluated by a receptor blocking study that utilized the pretreatment of Egen and incubation with targeted NPs. For the receptor blocking study, cells were treated with free Egen (2 mg/ml) before 6 h of the treatment with CM6-CS-g-Egen NPs. Finally, the cell monolayers were captured by using confocal microscopy [114].

3.4.4.5 *In vitro* cytotoxicity assay

The *in vitro* cytotoxicity activity of the free PLB, PLB-CS NPs and PLB-CS-g-Egen NPs were evaluated in the estrogen overexpressed breast cancer cell lines (T-47D and MCF-7). Briefly, 1×10^4 cells were seeded in each well of a 96 well cell culture plate in DMEM and maintained overnight in a CO_2 humidified incubator (5 %, CO_2) at 37° C. After overnight of the incubation, utilized media was eliminated and the cells were treated with a free drug, PLB-CS-g-Egen NPs at different concentrations (0.01 µg/ml, 0.1 µg/ml, 1

μg/ml, 10 μg/ml, and 100 μg/ml) diluted in DMEM medium and incubated for 24 h. After drug incubation, the containing medium was discarded, and fresh MTT containing medium was added to each well and incubated for 4 h. The treatment medium was gently shaken without disturbing the formazan crystal. Additionally, the crystals were washed and dried for an additional 2 h. Followed by washing and drying for another 2 h. Finally, 100 μl DMSO was added into each well and gently shaken on the gyratory shaker for 30 min, followed by the optical density of the samples were taken at 570 nm by using a microplate reader (Multiplate reader, BioRad) [114]. The percentage of cellular viability was estimated using the given formula.

$$\%\, Cellular\ viability\ = \frac{Absorbance\ of\ the\ treated\ cells}{Absorbance\ of\ the\ control\ cells} * 100$$

3.4.4.6 Apoptosis study with Hoechst/PI dual staining

The apoptotic potential of free drug and receptor mediated drug delivery was determined by the Hoechst 33342/PI dual stating method. Briefly, 1 ×10^5 MCF-7 and T-47D cells were seeded in 12 well cell culture plates, separately. Then, cells were treated with free PLB, PLB-CS NPs and PLB-CS-g-Egen NPs for 24 h at 37°C in CO_2. For the receptor blocking study, cells were treated with 2 mg/ml of free Egen prior to 6 h of PLB-CS-g-Egen NPs treatments. After 24 h of incubation, the drug containing medium was discarded and the cells were stained with a 10 μg/ml concentration of Hoechst/PI and incubated for 30 min. Then, the cells were washed with PBS and finally, images were taken by a fluorescence microscope (EVOS FL live cell imaging system) at 400X [115].

3.4.4.7 Cell cycle analysis

Cell cycle analysis of free PLB, PLB-CS NPs and PLB-CS-g-Egen NPs was performed in MCF-7 cell lines [116]. In brief, 1 × 10^5 MCF-7 cells were seeded in a six-well cell culture plate and allowed to grow. Then, cells were incubated separately with free

PLB, PLB-CS NPs, and PLB-CS-g-Egen NPs for 24 h. After incubation, the cells were harvested with 1 mM EDTA in cold PBS, followed by fixing them with 75% ethanol (ice cold). After fixation, the cells were kept at −20 °C overnight, and then, the cells were incubated with a mixture of 20 μg/mL of PI, 0.1% of Triton-X, and 200 μg/mL of RNase A. The stained cells were maintained at room temperature in the absence of light for 30 min prior to analysis. Finally, the cells were subjected to flow cytometry for the analysis (CytoFLEX S N2-V4-B2-Y4, Beckman Coulter, United States).

3.4.5 *In vivo* studies

3.4.5.1 Pharmacokinetic study

Female Sprague Dawley (SD) rats weighing 150−200 g and 45−60 days old were procured from the animal house of IMS BHU, India. All the experimental protocols related to the animal studies (three rats per group) were approved by the Institutional Animal Ethics Committee (IAEC), IIT BHU, India. All the rats were maintained at room temperature and supplied with water and standard rat feed under natural light/dark conditions for 1 week before experiments. All the rats were randomly segregated into four groups, and each group consisted of three animals (n = 3). The first group of rats was given blank NPs intravenously, the second group of rats was administered with an intravenous injection of free PLB (suspension in sterile normal saline), the third group of rats was administered with PLB-CS NPs, and the fourth group received PLB-CS-g-Egen NPs [102]. Prior to the intravenous injections, all the nanoparticles were passed through a 0.45 μm syringe filter followed by terminal sterilization under UV light for 2 h. Intravenous injection of the different formulations was given at a dose of 5.91 mg/kg body weight. Following the administration of the different formulations, 0.4 mL of blood from rats was collected in heparinized tubes under mild anesthetic conditions. The sampling time points of blood collection were 0.5, 1, 2, 4, 8, 12, 24, and 48 h. Plasma from each sample was separated by

centrifugation (5000 rpm, 5 min) at 4 °C. The plasma protein was precipitated by the addition of an equal volume of acetonitrile to the plasma samples. Further, samples were centrifuged at 15,000 rpm (10 min) to remove the precipitated protein. Finally, the supernatant was collected, filtered through a syringe filter, and analyzed by a validated HPLC method after suitable dilution with the mobile phase.

3.4.5.2 Histopathology study

The safety of the prepared formulations was analysed by histopathological study for reporting any toxicity that appeared after multiple administrations of the formulation to the rats (n=3). The PLB 5.91 mg/kg rat dose was fixed by considering the reported 125 mg of PLB adult dose, 46% oral bioavailability, and metabolic rate in the rats. The rats were randomly segregated into four groups, with three animals in each group. Intravenous injections of saline (vehicle control), free PLB (drug control), PLB-CS NPs (nontargeted NPs), and PLB-CS-g-Egen NPs (targeted NPs) were done at a dose of 5.91 mg/kg at an interval of 3 days. On the 15^{th} day, all rats were sacrificed, and vital organs (brain, lungs, liver, kidney, and spleen) were isolated. The organs were washed with normal saline and fixed in the mounting medium for cryostat. The samples were sectioned in a cryomicrotome (Leica CM1950) having 5 μm thickness. The sample sections were stained with hematoxylin and eosin (H & E) dye [117]. All the stained specimens were mounted on glass slides for visualization under a bright microscope and images were captured by using a Dewinter microscope (Capture Pro 4.1 software).

3.4.5.3 Animals

Female SD rats (150-200 g body weight, 45-60 days age) were maintained at room temperature under standard conditions and foods. IAEC, IIT BHU, Varanasi, India approved all the procedures performed on the animals.

3.4.5.4 Tumor induction

For the induction of the breast tumor, 5 mg of 7,12-dimethylbenz(a)anthracene (DMBA) was dissolved in 0.5 ml of vehicle (sunflower oil) and administered subcutaneously to the rat mammary pad one or either side. All rats were screened for the development of tumors at the beginning of the 8 weeks of DMBA treatment. The screening involves palpitation of the mammary pad for the development of any abnormal mass. Tumor yield and size were stabilized after 75 days (Approx.) of DMBA treatment [118-120]. Rats were kept palpitated, and tumor sizes were ranged from 5–8 mm were used for the *in vivo* anticancer activity. DMBA induced breast tumors are overexpressed with hormonal receptors such as (ER and PR) [121] and the cell line derived from the DMBA-induced breast tumors exhibits a similar nature to that of the MCF-7 cell line [122].

3.4.5.5 Histological identification of the tumor

The developed tumor from a rat (DMBA treated) was harvested and washed with normal saline. The tumor was fixed in the paraffin wax and 5 µm thick section was prepared by using a microtome. As of today, H & E staining is the gold standard technique for the differentiation of the tumor from the normal tissue. The obtained tumor section was stained with H & E stain as per the standard protocol, and a slide was prepared. Similarly, a normal rat breast pad was isolated, and H & E staining was performed for the comparison with breast tumor.

Additionally, the prepared paraffin block of the tumor was sectioned to get 5 µm thick tissue and treated with ER antibody as per the standard protocol of immunohistochemistry for the detection of the ER expression. The prepared specimen was subjected to the ER scoring. As per the College of American Pathologists (CAP) guideline for ER scoring, >1 % of immunoreactive tumor cells are positive for ER, whereas <1 % is considered negative [123].

3.4.5.6 *In vivo* antitumor study by ultrasound and photoacoustic imaging

Female SD rats with induced breast cancer were used for the *in vivo* antitumor study. Breast tumor induced rats were randomly distributed into four groups, each group containing 3 rats (n=3). All the animals breast tumor was scanned by using ultrasound and a photoacoustic imaging system (Vevo LAZR_X Vevo 3100 imaging system, Toronto, Canada) equipped with a 40-MHz ultrasound array transducer prior to the treatment with NPs. The scanning of the breast tumor was performed in B-mode (ultrasound mode), Power Doppler mode (for vascularity) and photoacoustic mode. All the animals received intravenous dosing of the free drug and NPs (5.91 mg/kg body weight). The first group (control) received no treatments, the second group received PLB (drug control), the hird group received PLB-CS NPs and the fourth group received PLB-CS-g-Egen NPs. Photoacoustic and ultrasound images of the breast tumors were visualized at 0 days, 2^{nd} days, 4^{th} days and 8^{th} days after the treatments. For the visualization of the tumor area in ultrasound and photoacoustic analysis mode, the tumor area was irradiated with 700 nm, 40 MHz pulse repetition frequency. The captured images of the ultrasound and photoacoustic were overlaid to determine the size, shape and oxygenation level of the tumor. Power Doppler images were analyses for checking tumor vascularity and angiogenesis. All the images were processed by using Vevo LAB software (FUJIFILM VisualSonics, Toronto, Canada).

3.4.5.7 *In vivo* breast tumor targeting efficiency by IVIS live imaging.

In vivo fluorescence imaging of free DiD (control), DiD-CS NPs, and DiD-CS-g-Egen NPs was performed on DMBA induced breast tumors in rats using the Photon Imager Optima System (Biospace Lab). The free DiD and DiD loaded NPs equivalent to 200 nM of DiD dye were administered intravenously by the tail vein to the rats, and the fluorescence signals were captured at excitation and emission wavelengths of 620 and 710

nm, respectively, at 2, 4, 6, and 8 h postinjection. The radiant efficiency (measured as fluorescence intensity/area/time) was analyzed using the Biospace Lab imaging software by the region of interest (ROI) tool the encircled the breast tumor area.

3.4.6 Statistical analysis

Data from the *in vitro* and *in vivo* experiments were presented as the mean ± S.D (n=3). The GraphPad Prism 7.0 was used for the statistical calculation. One way ANOVA and the t-test were used was to calculate the statistical significance among groups. The statistically significant level was considered as ns ($p \geq 0.05$), * ($p < 0.05$), ** ($p < 0.01$), *** ($p < 0.001$) and **** ($p < 0.0001$).

3.5 Results and discussion

3.5.1 Characterization of CS-g-Egen conjugate

3.5.1.1 FTIR

The FTIR spectra of CS, Egen, Egen-COOH, and CS-g-Egen were compared to analyze the synthesized Egen-COOH and CS-g-Egen, as shown in **figure 3.2**. Egen demonstrated the FTIR peaks of OH, C−H, C=O (ketone), C−O, and C=C (aromatic) stretching peaks at 3360, 2909, 1718, 1240, and 1556 cm^{-1}. Egen-COOH showed OH, C−H, C=O (ester), C−O, and C=C (aromatic) stretching vibrations at 3303, 2943, 1725, 1285, and 1658 cm^{-1}, respectively. A slight shift in the FTIR peak of Egen was observed after carboxylation and formation of the ester bond. Meanwhile, CS-g-Egen demonstrated OH, C−H, C=O (amide), C−O, and C=C (aromatic) stretching vibrations at 3360, 2898, 1678, 1217, 1048, and 1556 cm^{-1}, respectively, and NH bending vibrations at 1624 cm^{-1}. When Egen-COOH was conjugated with CS, the formation of the amide bond was observed, which led to a slight shift in the FTIR peaks. **Table 3.2** shows all the characteristic peaks related to their functional groups.

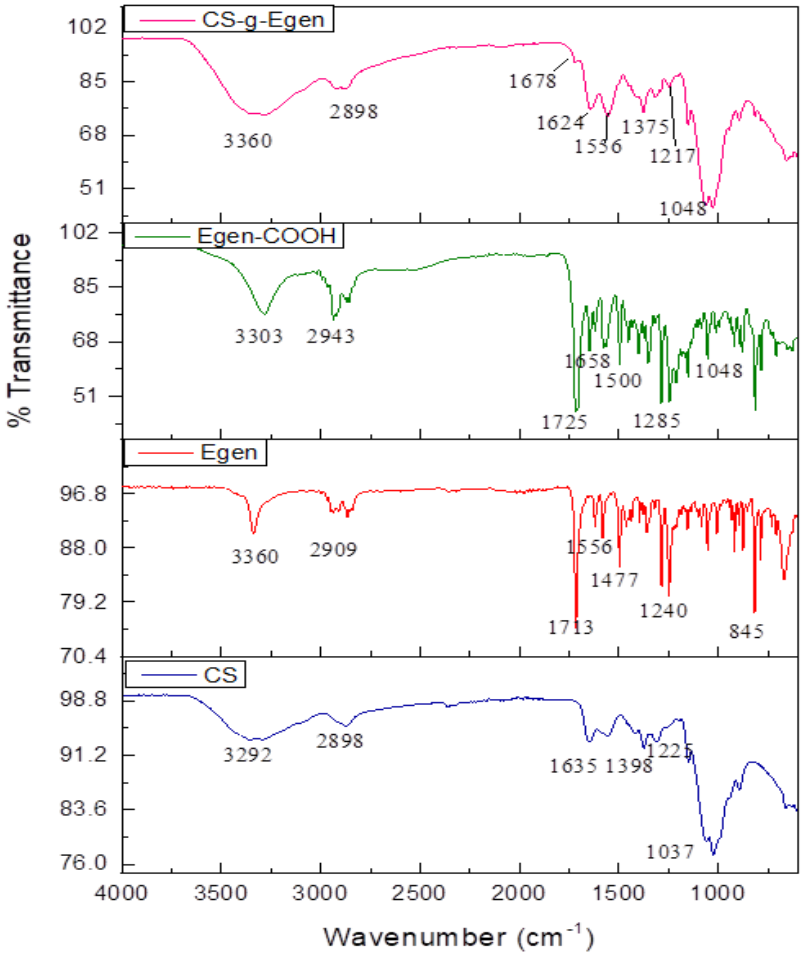

Figure 3.2 FTIR-ART spectra of the chitosan, Egen, Egen-COOH and CS-g-Egen

Table 3.2 FTIR peak assignment of CS, Egen, Egen-COOH, and CS-g-Egen

Peak Assignment	Wavenumber (Cm^{-1})			
	CS	Egen	Egen-COOH	CS-g-Egen
OH stretch	3392 (broad)	3360	3303	3360
NH bending	1635	-	-	1624
C-H stretching	2898	2909	2943	2898
C=O stretching	-	1718 (ketone)	1725 (ester)	1678 (amide)
C-O stretching	1225	1240	1285	1217
C-O-C stretching	1137	-	-	1048
Aromatic C=C stretching	-	1556	1658	1556

3.5.1.2 NMR

Figure. 3.3 displayed the ^{1}H-NMR spectra of CS, Egen, Egen-COOH and CS-g-Egen. The spectra of CS displayed the peak of the NH_2 functional group at 1.8-2 ppm,

whereas these peaks were absent in the spectra of Egen-COOH due to the substitution. However, the spectra of Egen-COOH also displayed the peaks of methylene protons of the conjugated succinate group at 3 ppm and aromatic protons of estrogen at 6.5 ppm and 7 ppm. Moreover, the spectra of CS-g-Egen consist of the characteristic peak NH of the amide linkage at 8.3 ppm and aromatic protons at 6.5, 7 and 7.6 ppm. All these findings support the successful conjugation of CS-g-Egen.

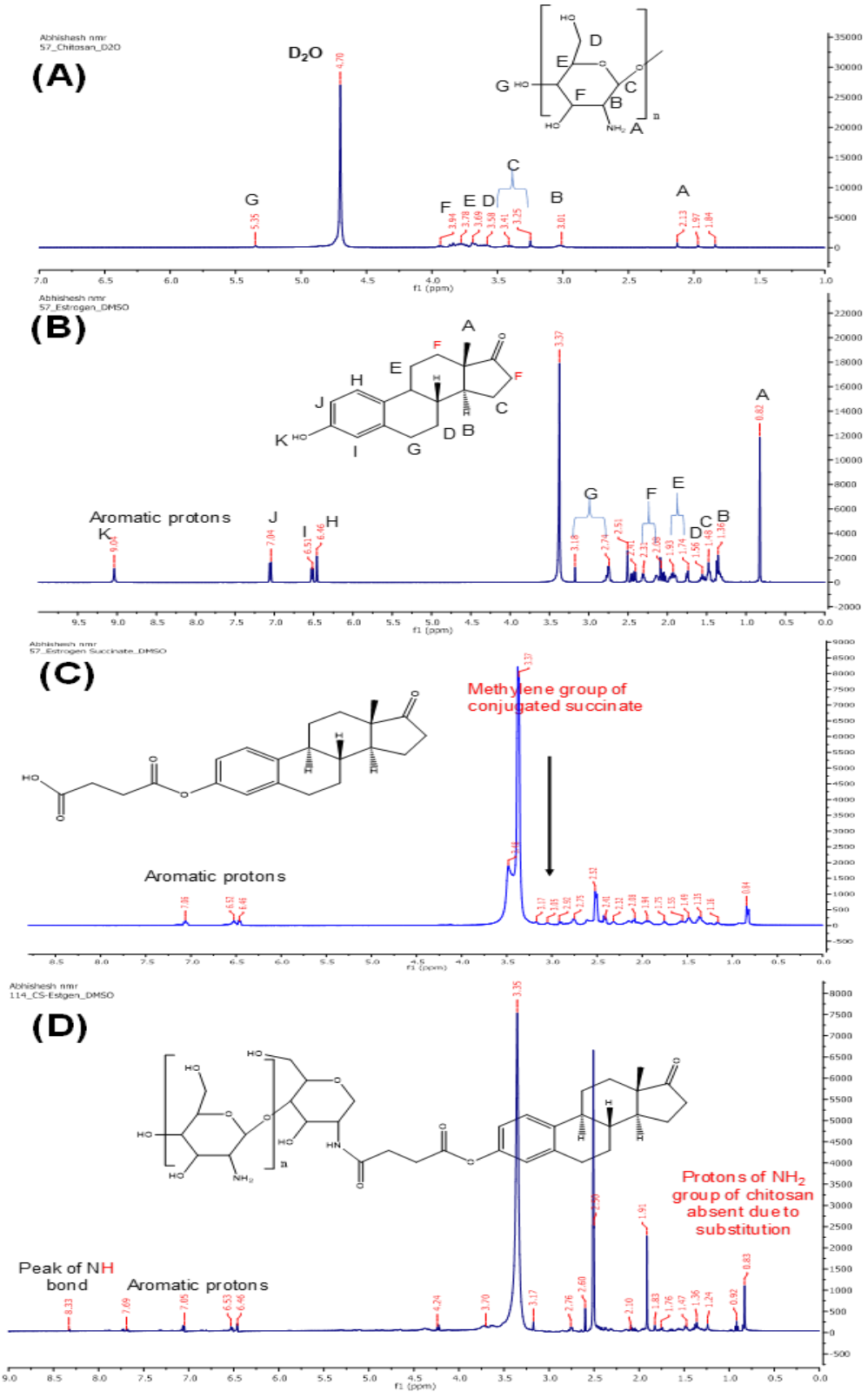

Figure 3.3 NMR spectra of A) CS, B) Egen, C) Egen-COOH and D) CS-g-Egen

3.5.1.3 High resolution mass spectroscopy

The synthesized Egen-COOH and its conjugate with CS (CS-g-Egen) were examined by time of flight mass spectroscopy (**Figure 3.4. A, A1, A2, and B**).

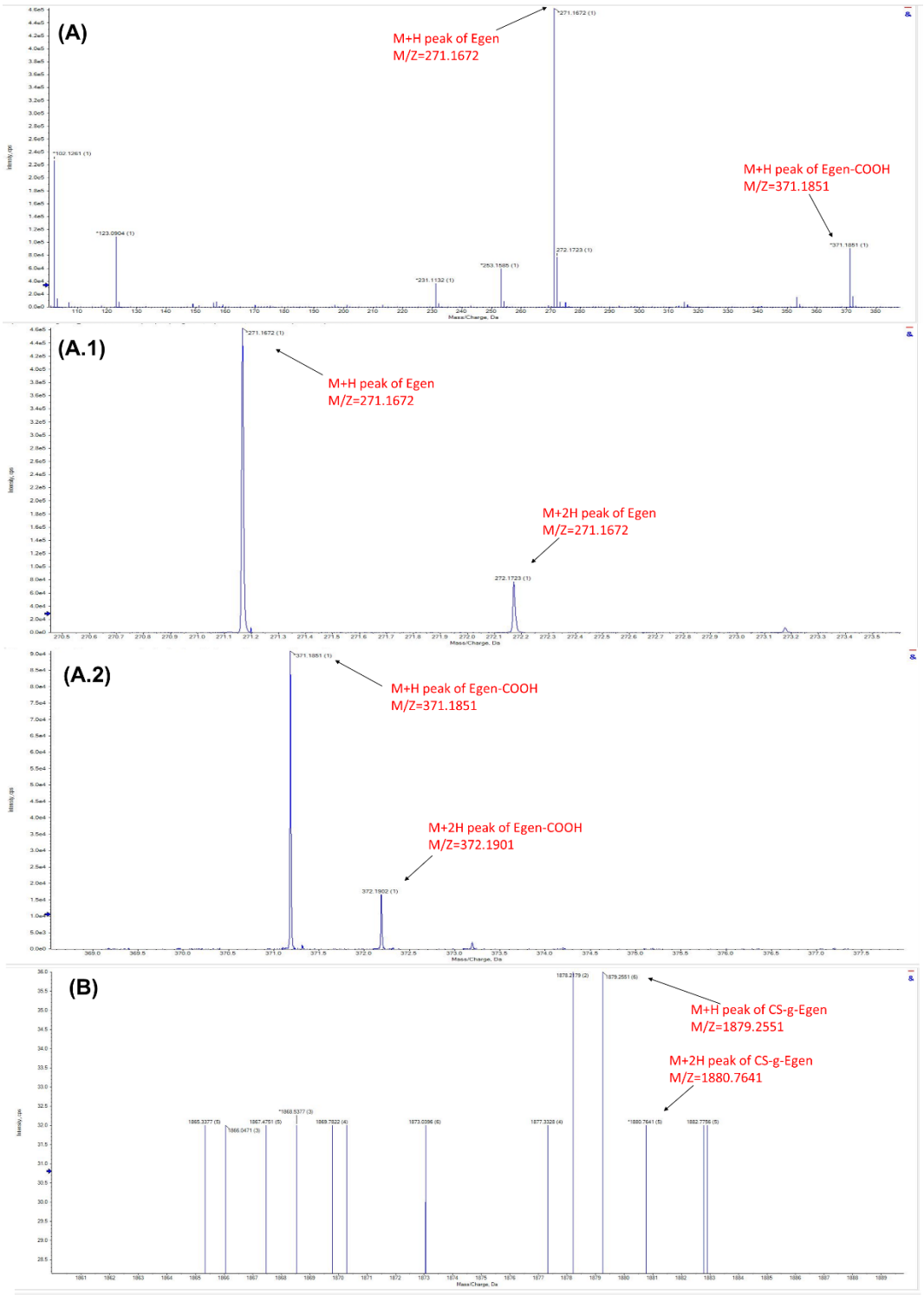

Figure 3.4 HRMS spectra of A) Egen-COOH showing M+H peak of Egen and Egen-COOH, A.1) showing M+H peak of Egen, A.2) showing M+H & M+2H peak of Egen-COOH B) CS-g-Egen.

The Egen was functionalized with –COOH by the process of succinylation. The molecular weight of Egen was 270.4 g/mol and after succinylation, it was increased to 370.4 g/mol. The molecular ion peaks of the Egen-COOH (M+H) was at m/z of 371.18 (**Figure 3.4, A**) and the M+2H peak was observed at an m/z of 372.19 (**Figure 3.4, A2**). The formation of the amide linkage between the carbonyl carbon of Egen-COOH and an amino group of CS releases a molecule of water. The molecular weights of CS and Egen-COOH are 1526.5 g/mol and 370.4 g/mol, respectively. The molecular weight of the CS-g-Egen was approximately 1878.9 g/mol and the molecular ion peaks (M+H and M+2H) in the spectra of the CS-g-Egen appeared at m/z 1879.25, and 1880.76, respectively. The HRMS analysis (**Figure 3.4**) demonstrated the successful formation of the Egen-COOH and conjugation of the CS with Egen to form the CS-g-Egen graft polymer.

3.5.1.4 Degree of Egen substitution

The degree of the substitution of the Egen to the CS was found to be 0.82 ± 0.02. The degree of conjugation can be maximum up to 1, which indicates one molecule of the Egen successfully substituted on the one molecule of the CS. In this case, we obtained 0.82, which suggests that 82 % of the CS molecules have Egen substitution.

3.5.2 Nanoparticles characterization

3.5.2.1 PS, PDI, and ZP of NPs

The characterization of the NPs is presented in **Table 3.3**. The developed NP showed hydrodynamic diameters ranging from 101.2 ± 2.73 nm to 141.6 ± 1.97 nm. The obtained particle size data demonstrated that developed NPs were in the range of 100 to 150 nm in size. The blank CS NPs were found to have a size of 101.2 nm and a zetapotential of 19.90 mV, whereas PLB loading has significantly ($P<0.001$) increased the particle size (116.3 nm) and caused a slight reduction ($p>0.05$, ns) in the zetapotential (18.70 mV) of nontargeted NPs due to entrapment of the PLB in the polymeric matrix of CS. Additionally,

in the case of targeted NPs, incorporation of the CS-g-Egen has significantly($P<0.001$) increased the particle size (141.6 nm) and reduced the zetapotential (12.45 mV).

Table 3.3 PS, PDI, ZP, EE and IC50 value of developed NPs

Batches	PS nm (mean ± S.D*)	PDI (mean ± S.D*)	ZP (mV) (mean ± S.D*)	EE (mean ± S.D*)	IC_{50} (µg/ml) (mean ± S.D*)	
					MCF-7	T-47D
PLB	-	-	-	-	41.86±1.53	48.32±1.296
Blank CS NPs	101.2 ± 2.73	0.198± 0.058	19.90± 0.568	-	-	-
PLB-CS NPs	116.3 ± 1.53	0.240± 0.032	18.70± 0.416	72.93± 1.297	3.45±0.45	6.29±0.67
PLB-CS-g-Egen NPs	141.6± 1.97	0.220±0.042	12.45±0.574	75.79± 2.195	0.73±0.07	1.59±0. 08
CM6-CS NPs	110.2± 1.27	0.240±0.022	17.20± 0.354	86.69± 1.675	-	-
CM6-CS-g-Egen NPs	135.3± 1.41	0.250±0.014	11.38±0.251	84.47± 2.161	-	-

*n = 3; S.D: Standard deviation
Blank CS NPs: Blank chitosan nanoparticles
PLB-CS NPs: Non-targeted PLB loaded chitosan nanoparticles
PLB-CS-g-Egen NPs: Estrogen receptor targeted PLB loaded chitosan nanoparticles
CM6-CS NPs: Non-targeted coumarin-6 loaded chitosan nanoparticles
CM6-CS-g-Egen NPs: Estrogen receptor targeted coumarin6 loaded chitosan nanoparticles
PS: particle size, PDI: Polydispersity index, ZP: zeta potential and EE: entrapment efficiency

The increase in size was attributed to the presence of the Egen (targeting moiety) on the NPs surfaces, whereas the decrease ($P<0.001$) in the zetapotential was mainly due to the presence of the low number of free NH_2 compared to nontargeted NPs. A statistical comparison of PLB, PLB-CS NPs, and PLB-CS-g-Egen NPs particle size and zetapotential has been presented in **Figure 3.5 (A & B).**

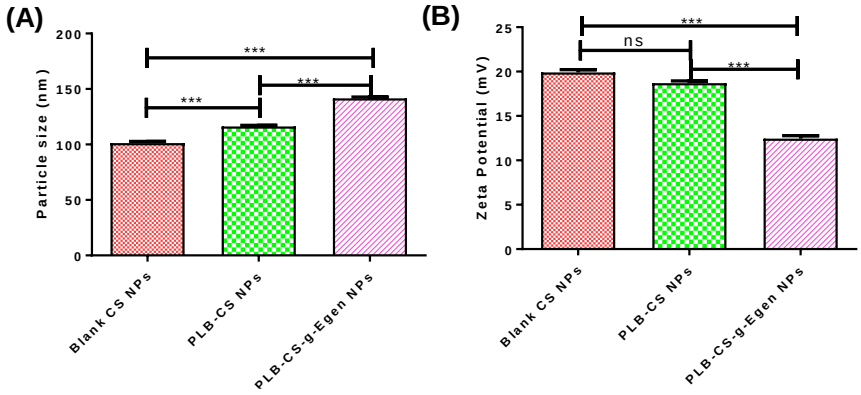

Figure 3.5 Statistical comparison of PLB, PLB-CS NPs, and PLB-CS-g-Egen NPs (A) particle size and (B) zetapotential.

3.5.2.2 Determination of entrapment efficiency

The amount of drug entrapped into the PLB-CS NPs and PLB-CS-g-Egen NPs were 72.93± 1.997 % and 75.7 9± 2.195 %, respectively (Table 2). Preconjugation of Egen did not significantly impact the EE of the targeted NPs. Similarly, EE of the CM6 in the CM6-CS NPs and CM6-CS-g-Egen NPs was found to be 86.69± 1.675 % and 84.47± 2.161 %, respectively. The entrapment of the PLB or CM6 in the nontargeted NPs and targeted NPs was not significantly different ($p \geq 0.05$).

3.5.2.3 FE-SEM

The morphology of the prepared NPs was analyzed by FE-SEM (FEI Pvt. Ltd., USA) and images were captured for the PLB-CS NPs and PLB-CS-g-Egen NPs. **Figure 3.6A** demonstrates developed NPs have spherical morphology, smooth texture, and uniformly dispersed particles. Targeted NPs were slightly bigger in size compared to the nontargeted NPs. Additionally, nontargeted NPs had completely smooth surfaces, whereas targeted NPs showed slightly rough surfaces, which may be due to the presence of Egen on the surface of the targeted NPs [124].

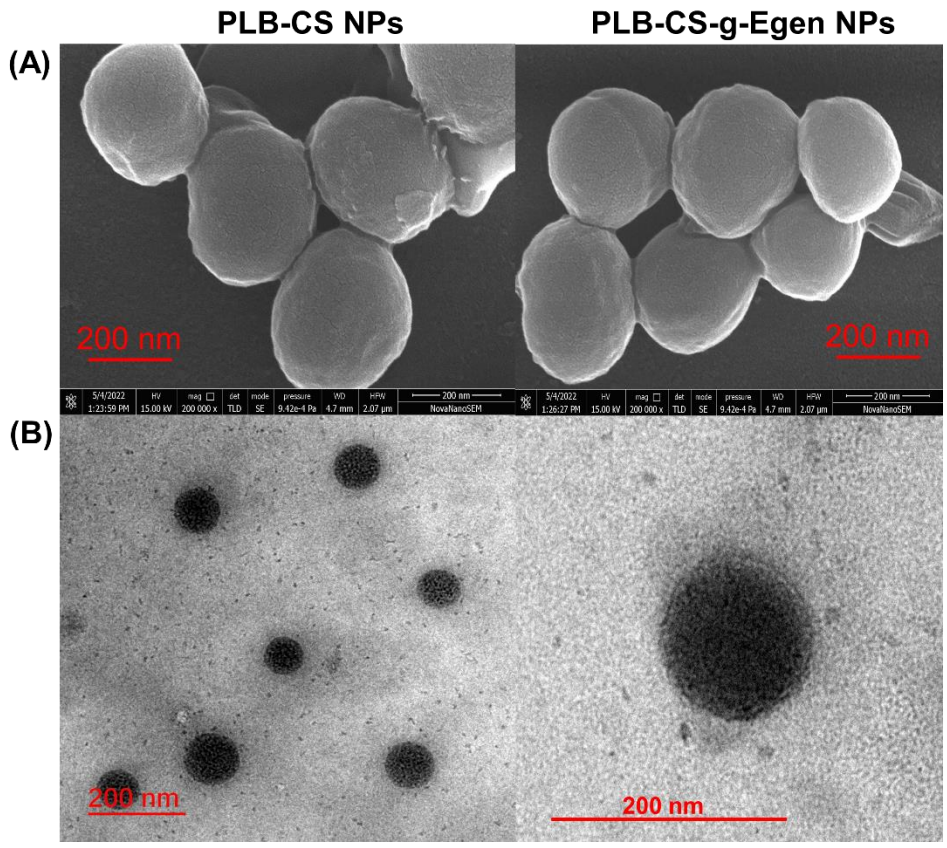

Figure 3.6 Morphological imaging of the PLB-CS NPs and PLB-CS-g-Egen NPs by (A) field emission scanning electron microscope (FE-SEM), (B) transmission electron microscope (TEM).

3.5.2.4 TEM

TEM uses an electron beam to capture the images of the NPs. These techniques provide a higher resolution of the images. **Figure 3.6B** depicts TEM images of NPs with a 200 and 100 nm scale. Images of nontargeted and targeted NPs showed a completely spherical shape.

3.5.2.5 AFM

AFM provides two-dimensional (2D) and three-dimensional (3D) topography of the NPs. It is non-optical imaging technique that provides high resolution images of the NPs. The 2D and 3D AFM images in **Figure 3.7A and B** showed that nontargeted NPs and targeted NPs were spherical in shape with uniform particle size distribution. Additionally, targeted NPs appear to be slightly bigger in size compared to the nontargeted NPs.

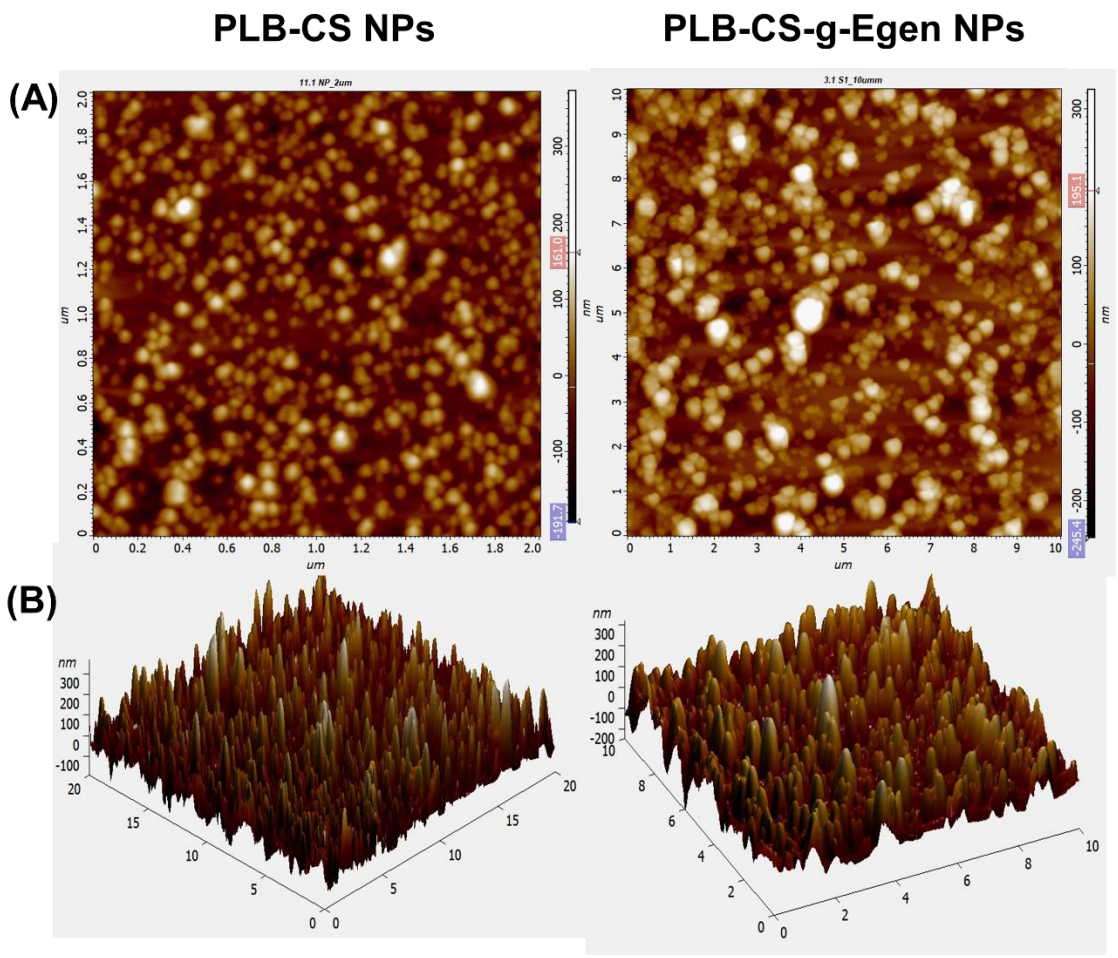

Figure 3.7 (A) two dimensional atomic force microscope (AFM) and (B) three-dimensional AFM.

3.5.3 Surface chemistry by XPS

X-ray photoelectron spectroscopy (XPS) was used to investigate the surface chemistry of PLB-CS NPs and PLB-CS-g-Egen NPs. The atomic signal of C, N, and O from NPs in terms of the XPS peak has been presented in **Figure 3.8A**. In the XPS survey, C1s, N1s, and O1s were detected at the binding energy of 250-300 eV, 400-450 eV, and 500-550 eV, respectively. The atomic percentage of C1s, N1s, and O1s in the nontargeted NPs was found to be 76.86 %, 2.95 %, and 20.19 %, respectively, whereas targeted NPs showed a peak of C1s, N1s and O1s as 73.52 %, 1.51 % and 24.97 %, respectively. The decrease in the nitrogen atomic percentage in the PLB-CS-g-Egen NPs was due to the pre-conjugation of the free nitrogen of the CS with Egen and, hence, the availability of the nitrogen atom on the surface of the PLB-CS-g-Egen NPs were lesser than PLB-CS NPs.

Additionally, an increase in the O1s signal in the targeted NPs again confirmed the presence of the Egen on the targeted NPs surface, mainly due to the presence of oxygen in the structure of the Egen-COOH.

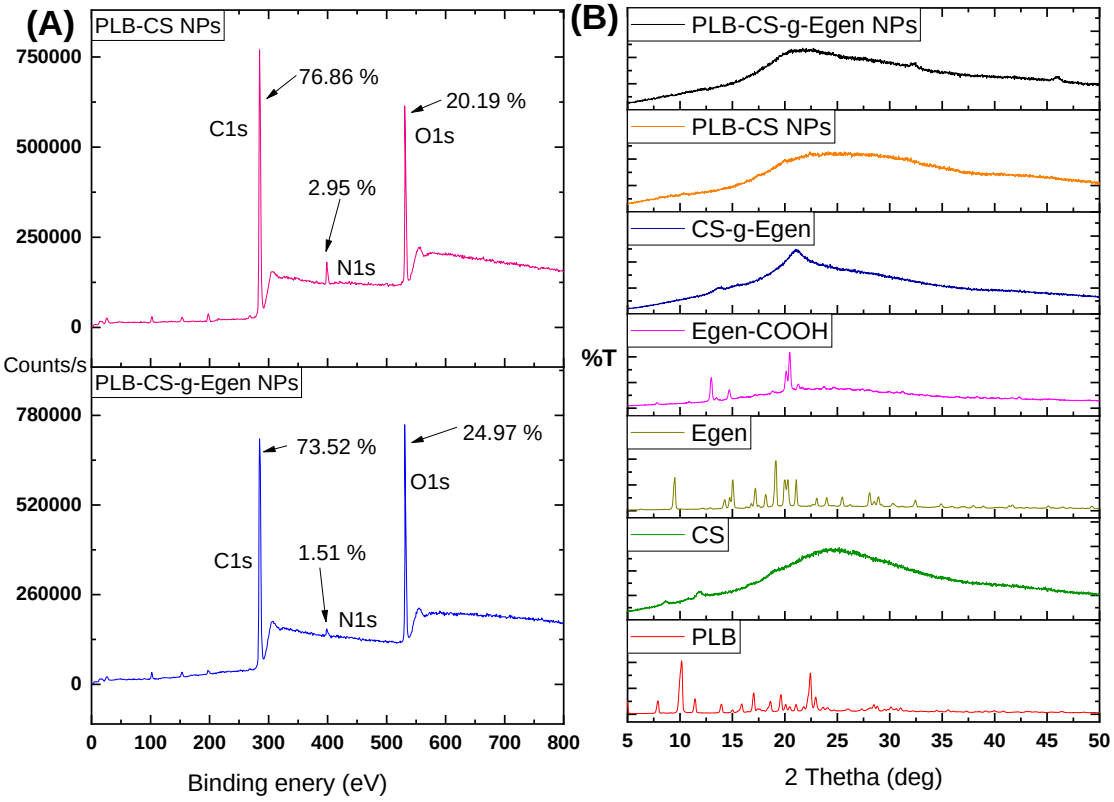

Figure 3.8 A) X-ray photoelectron spectroscopy (XPS) analysis of PLB-CS NPs and PLB-CS-g-Egen NPs, B) X-ray diffraction (XRD) spectra of the PLB, CS, Egen, Egen-COOH, CS-g-Egen, PLB-CS NPs and PLB-CS-g-Egen NPs.

3.5.3.1 Egen surface content

The quantity of Egen present on the surface of the PLB-CS-g-Egen NPs was found to be 71.2 ± 2.0 %. The surface content of the Egen is essential for the targeted delivery of the PLB via receptor mediated endocytosis of the PLB-CS-g-Egen NPs.

3.5.3.2 XRD study

An XRD study provided an understanding of the physical state of the drug in the formulation. Any changes in the physical state of the drug during formulation of the NPs can be tracked by using XRD analysis. Drugs either exist in crystalline or amorphous form; the amorphous form of the drug has good solubility and higher bioavailability compared to

the crystalline counterpart [125]. The XRD data of PLB showed sharp multiple diffracted peaks at 2θ=7.83°, 10.19°, 11.35°, 13.86°, 17.07°, 18.64°,19.86°, 21.15°, 22.48° and 22.95°. Pure PLB exists in the crystalline form (**Figure 3.8B**) and which is in good agreement with previously reported data [126]. All the PLB peaks were absent in the nontargeted and targeted NPs, suggesting that the drug has converted into an amorphous form following the NPs preparations. Hence, the developed formulation was found to have amorphous solid dispersion of the PLB inside the NPs. The amorphous form of the PLB has higher bioavailability relative to its crystalline form and hence may enhance the bioavailability of the PLB following NPs preparation. Crystalline nature of the Egen has reduced after conversion into Egen-COOH and further reduced after conjugation of CS. CS and CS-g-Egen polymer exist as amorphous form as depicted in their XRD graph.

3.5.4 *In vitro* studies

3.5.4.1 *In vitro* drug release studies

In vitro drug release profile of PLB-CS NPs and PLB-CS-g-Egen NPs at pH 5.5 and pH 7.4 has been presented in **figure 3.9.** The physiological pH normal huma system is pH 7.4, whereas the tumor microenvironment has acidic pH (below 6.0) [127, 128]. T_{50} is the time at which 50 % of the loaded drug is released in the medium under a given set of conditions.

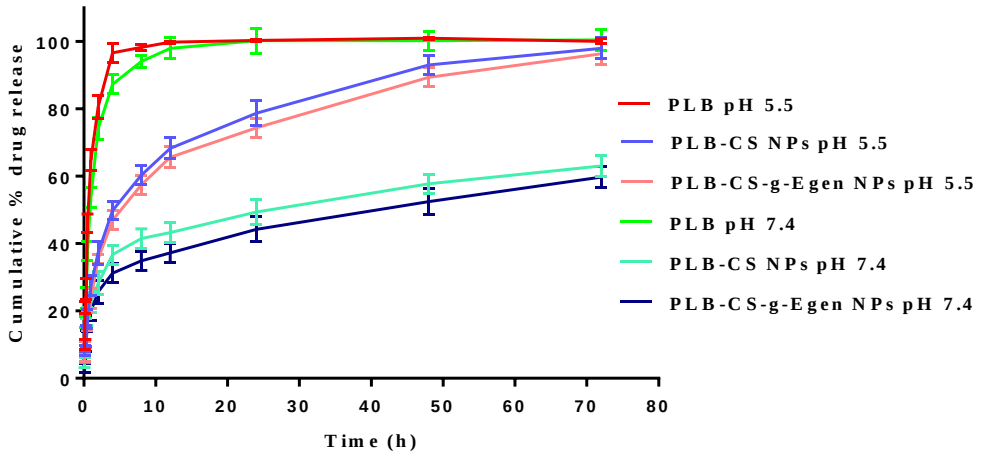

Figure 3.9 *In vitro* drug release profile of the PLB and NPs formulations in the pH 5.5 acetate buffer and pH 7.4 phosphate buffer saline.

The T_{50} value of the PLB, nontargeted, and targeted NPs in pH 5.5 was found to be 0.55 ± 0.05 h, 4.04 ± 0.22 h, and 5.97 ± 0.27 h, respectively. Whereas the T_{50} value of the PLB, nontargeted, and targeted NPs in pH 7.4 was found to be 0.83 ± 0.04 h, 25.20 ± 0.5 h, and 40.80 ± 0.6 h, respectively. The T_{50} value of PLB was significantly ($P<0.001$) lower than that of targeted and nontargeted NPs at pH 5.5 and pH 7.4. **Figure. 3.10 (A & B)** presents a statistical comparison of PLB, PLB-CS NPs, and PLB-CS-g-Egen NPs T_{50} at pH 5.5 and pH 7.4.

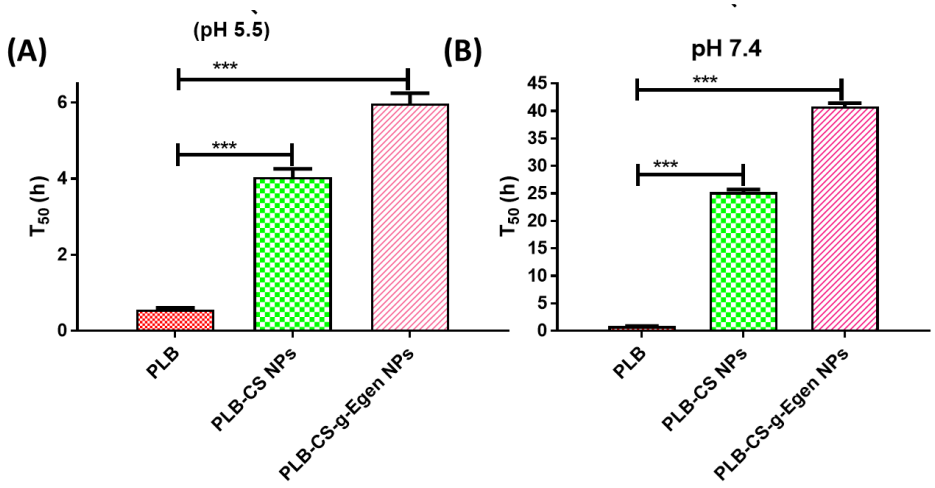

Figure 3.10 Statistical comparison of PLB, PLB-CS NPs, and PLB-CS-g-Egen NPs (A) T_{50} at pH 5.5 and (B) T_{50} at pH 7.4.

The release profile of PLB-CS NPs and PLB-CS-g-Egen NPs have demonstrated the pH dependent drug release profile. Nontargeted and targeted NPs demonstrated faster drug release at pH 5.5, which may be due to the protonation of the CS amino group increasing its aqueous solubility and drug releasing medium can easily diffuse into the NPs and promoting drug release faster. Whereas at pH 7.4 protonation CS was not feasible and hence NPs structure remains compact and hence diffusion of the drug from NPs occurs slowly. Free PLB release faster in the both medium due to absence of any controlling barrier except dialysis membrane. The NPs demonstrated initial burst release up to 2h, which may be due to the release of drug adhered to the NPs surface and faster diffusion drug present just beneath the NPs surface. Later on, sustained release of PLB may be attributed to the slower diffusion of the drug from the NPs inner part and core. PLB is distributed into the NPs polymeric matrix, and hence, the drug may take a longer time to reach the NPs surface.

Moreover, pH responsive release patter of the NPs at pH 5.5 (faster release) can be favorable for treating tumors due to its acidic microenvironment [129].

3.5.4.2 Hemolysis and hemocompatibility study

3.5.4.2.1 Blood smear

Nanoscale materials fall within the spectrum of viral sizes, and immunogenic proteins can stimulate the immune system, trigger an inflammatory process and change hematological parameters [130]. We performed a hematological analysis to observe any potential toxicity of the PLB, PLB-CS NPs and PLB-CS-g-Egen NPs. In this study, deionized water was taken as a positive control, which causes 100 % hemolysis, and normal saline (pH 7.4) was used as a negative control (nonhemolytic). The blood samples were treated with different formulations and stained with Leishman stain for visualization under a bright microscope (**Figure 3.11C)** at a resolution of 40X. The obtained images depicted

that treatment with PLB, PLB-CS NPs and PLB-CS-g-Egen NPs did not significantly affect the morphology of the blood cells and was similar to the saline-treated samples.

3.5.4.2.2 Hemolytic assay

The hematological safety of the PLB, PLB-CS NPs and PLB-CS-g-Egen NPs was analyzed by calculating the % of hemolysis that occurred after treatment with different formulations. Hemolysis % of PLB, PLB-CS NPs and PLB-CS-g-Egen NPs were 3.761 ± 0.07 %, 2.035 ± 0.04 %, and 1.718 ± 0.10 %, respectively. The results (**Figure 3.11B**) demonstrated that PLB, nontargeted, and targeted NPs were nonhemolytic to human blood [131].

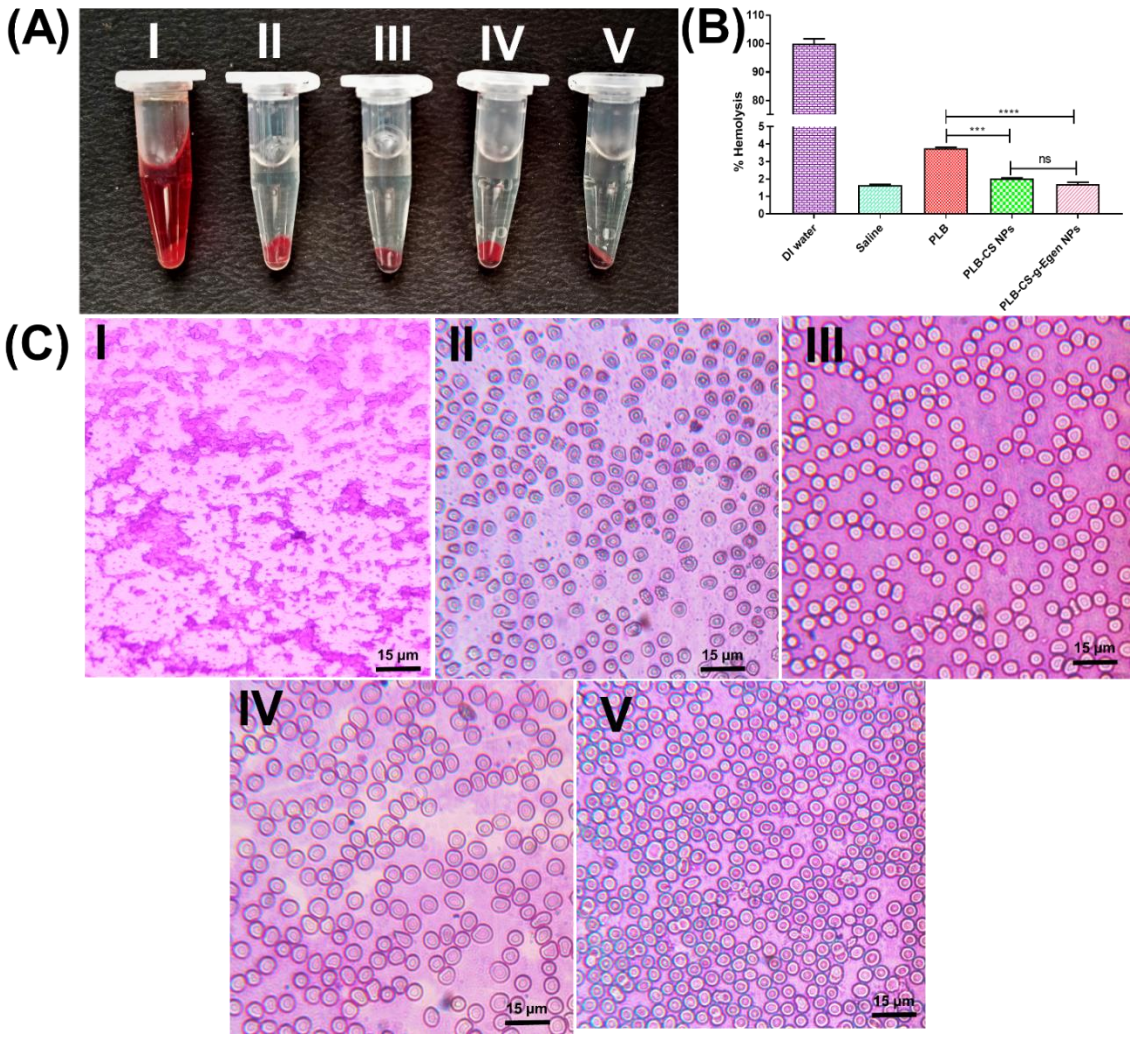

Figure 3.11 (A & B) Hemolysis study; I) Distilled water, II) Saline, III) PLB, IV) PLB-CS NPs, V) PLB-CS-g-Egen NPs and (C) hemocompatibility study; I) Distill water, II) Saline, III) PLB, IV) PLB-CS NPs, V) PLB-CS-g-Egen NPs.

3.5.4.3 Cellular uptake study

Cellular uptake is a key parameter for the prediction or estimation of the therapeutic efficacy of the NPs. To enhance the cellular internalization of the NPs into the ER positive breast tumor, active targeting via receptor mediated endocytosis has been utilized in this study. CM6 is the model dye used for the study of the NPs cellular uptake of the cancer cell line. The incubation of the CM6, CM6-CS NPS, and CM6-CS-g-Egen NPs with MCF-7 cells and T-47D cells at an equivalent dose of 5 µg/ml of CM6 demonstrated that nontargeted and targeted NPs have higher cellular uptake compared to the free CM6 **(Figure 3.13)**. Additionally, targeted NPs have significantly higher fluorescence relative to

nontargeted NPs suggesting that receptor mediated cellular uptake of the Egen functionalized targeted NPs. The overexpressed mER is present on the cell membrane of MCF-7 cells and T-47D cells, whereas ERα and ERβ predominantly present in the cellular cytosol or nucleus [132, 133]. Nontargeted NPs were internalized by cells via passive uptake that includes adhesion of the NPs (CS is positively charged) to the negatively charged cancer cells and internalization of the NPs. Additionally, nontargeted NPs show enhanced permeation and retention effects due to leaky blood vessels in the tumor microenvironments. Moreover, the functionalization of Egen on targeted NPs has added the value of receptor mediated transcytosis and passive diffusion. Nontargeted NPs were internalized into the MCF-7 cells & T-47D cells and localized in the cytoplasm of the cells (**Figure 3.13**, second row), whereas targeted NPs demonstrated enhanced cellular internalization due to the presence of mER, ERα, and ERβ. Targeted NPs also demonstrated nuclear uptake of the NPs due to ERα and ERβ mediated cellular uptake (**Figure 3.13**, third row). Further, receptor blocking of the MCF-7 cells and T-47D with free Egen demonstrated reduced cellular uptake of the targeted NPs that confirmed the receptor-mediated cellular uptake of the CM6-CS-g-Egen NPs.

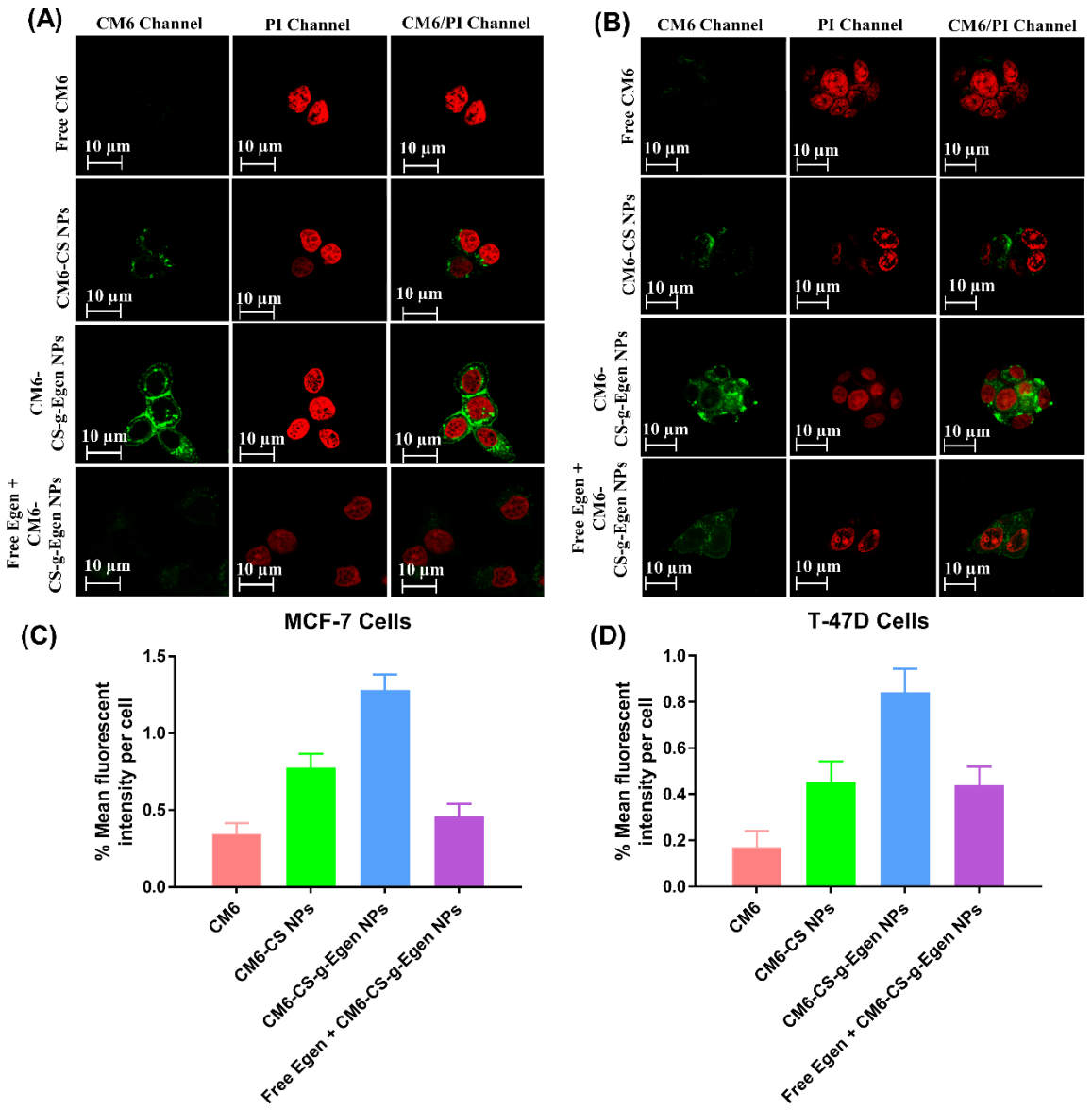

Figure 3.12 Confocal laser scanning microscopy (CLSM) images demonstrating cellular uptake of the free CM6 (first row), CM6-CS NPs (second row), CM6-CS-g-Egen NPs (third row), and CM6-CS-g-Egen NPs after pretreatment with Egen (fourth row) in (A) MCF-7 cells and (B) T-47D cells. The left column (CM6 channel) shows green fluorescence of CM6 distributed in the cytoplasm of (A) MCF-7 cells & (B) T-47D cells, the middle column (PI channel) shows red fluorescence from PI stained nucleus and the right column (merged) shows the CM6, CM6 loaded NPs, and PI stained nucleus. % Mean fluorescent intensity (green channel) in (C) MCF-7 cells and (D) T-47D cells after cellular uptake of CM6, CM6-CS NPs and CM6-CS-g-Egen NPs.

3.5.4.4 *In vitro* cytotoxicity assay

The obtained result shows that pure drug (palbociclib) does not induce any significant change in cell viability at lower concentrations, while their encapsulation in a nanoparticle system increases their efficacy by 12.13 folds in MCF-7 cells. Further, receptor mediated drug delivery of NPs was found to be most effective as compared to

nanoparticle mediated drug delivery (without receptor targeting). The IC_{50} value of PLB was found at ~41.86 µg/ml while PLB-CS NPs were found at ~3.45 µg/ml while receptor mediated targeting of cancer cells was found most effective, the IC_{50} value of PLB-CS-g-Egen NPs was found at ~0.73 µg/ml, concentration in MCF-7 cells **(Figure 3.13A & B)**. In T-47D cells, the IC_{50} of PLB was found at ~48.32 µg/ml, while IC_{50} of PLB-CS NPs was found at ~6.29 µg/ml. Further, IC_{50} of PLB-CS-g-Egen NPs, was found at ~1.59 µg/ml **(Figure 3.13C & D)**. So, on the basis of the obtained result, it can be concluded that the inclusion of receptor targeting moiety in the nanoparticle system increases the potential of the drug and makes it more than ~57 fold effective. MCF-7 and T-47D cells are overexpressed with ERs, receptor mediated targeted PLB delivery can significantly boost the anticancer efficacy of the PLB.

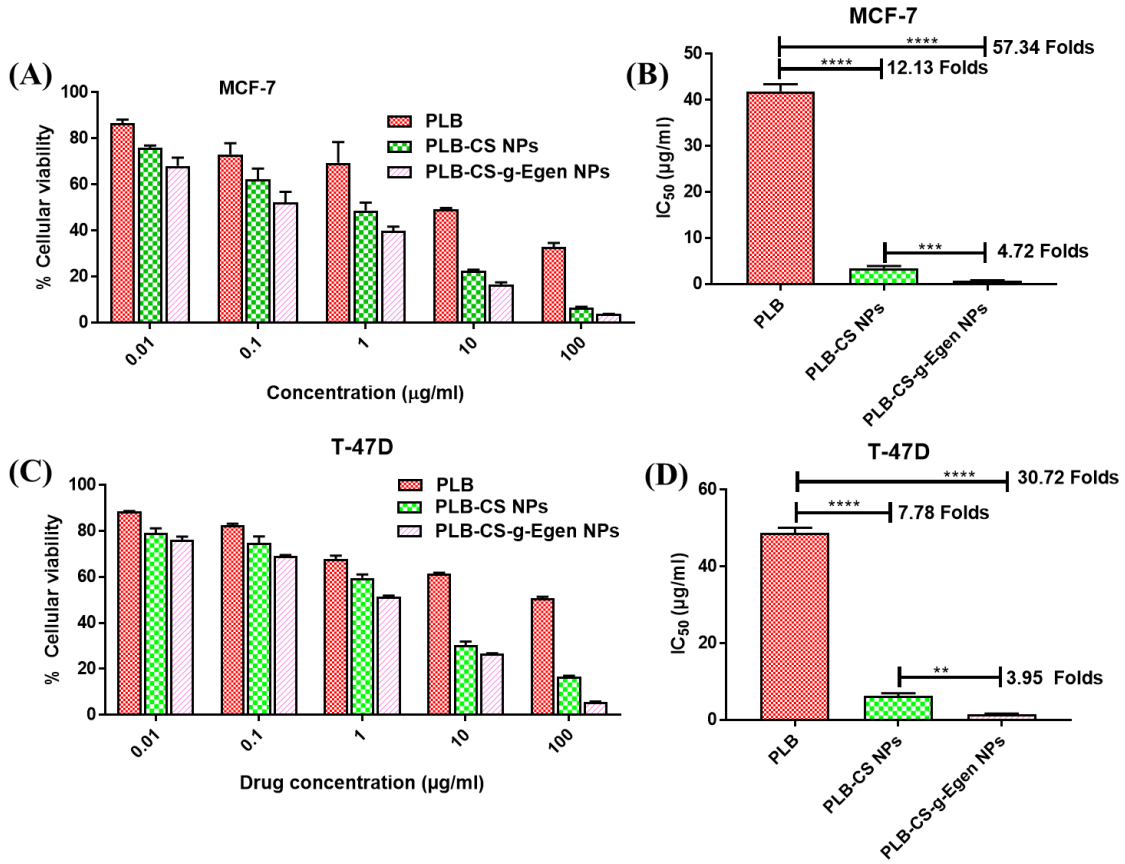

Figure 3.13 Cellular cytotoxicity assessment of the PLB, PLB-CS NPs and PLB-CS-g-Egen NPs on MCF-7 cells (A & B) and T-47D cells (C & D).

3.5.4.5 Hoechst/PI dual staining for apoptosis

Chromatin condensation, nuclear DNA fragmentation and cellular membrane blebbing are major the hallmarks of apoptosis after anticancer drug treatment [134]. In this study, we have used Hoechst and PI to stain the nuclei of the cells after PLB, PLB-CS NPs, and PLB-CS-g-Egen NPs treatments. Hoechst 33342 is a vital dye that stains the nuclei of both live and apoptotic cells, while PI only enters the cells with compromised cellular membranes [135]. Hoechst stains the condensed chromatin more brightly in apoptotic cells compared to normal cells. The staining patterns resulting from the simultaneous use of these dyes help differentiate the normal cells and apoptotic cells by using a fluorescence microscope or flow cytometer. After incubation, the MCF-7 cells and T-47D cells with PLB do not significantly induce apoptosis. Targeted NPs have significantly promoted apoptosis in MCF-7 and T-47D cells compared to nontargeted NPs due to receptor-mediated (mER, ERα, and ERβ) endocytosis of the NPs, which is also evident from the MTT assay and cellular uptake study.

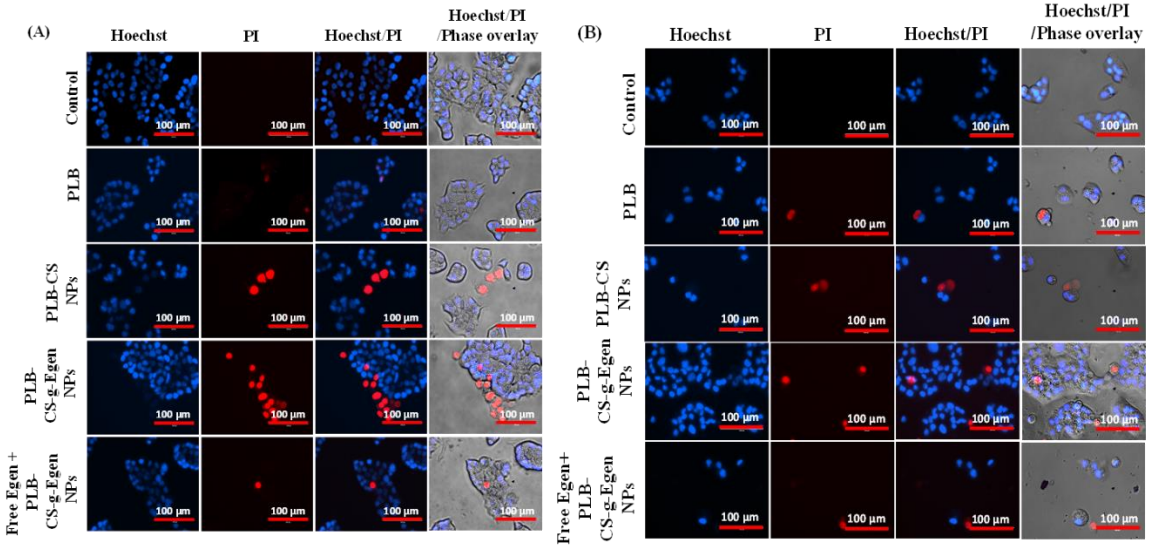

Figure 3.14 Apoptosis study of PLB, PLB-CS NPs, and PLB-CS-g-Egen NPs in (A) MCF-7 cells and (B) T-47D cells.

Additionally, receptor mediated cellular internalization was further confirmed by blocking or saturating the ER of cells with free Egen and treating cells with targeted NPs.

The obtained results demonstrated that a smaller number of apoptotic cells were observed in receptor blocked group of cells after treatment with targeted NPs. Moreover, targeted NPs demonstrated a higher number of apoptotic cells in MCF-7 cells compared to the T-47D cells. **Figure 3.14A**. represents the apoptosis study of PLB, PLB-CS NPs and PLB-CS-g-Egen NPs in MCF-7 cells, whereas **Figure 3.14B** presents the apoptosis study in the T-47D cells.

3.5.4.6 Cell cycle analysis

Further, the process by which drug and drug loaded NPs inhibit the growth of MCF-7 has been confirmed by flow cytometry analysis. PLB is a reversible inhibitor of CDK4/6, it inhibits the phosphorylation of the retinoblastoma (Rb), leading to the blocking of cell cycle progression from G1 to S phase. After treatment of the MCF-7 cells with PLB, PLB-CS NPs and PLB-CS-g-Egen NPs, PI stained cells were analyzed in a flow cytometer. The obtained data were processed by Cytoflex software. The nontargeted and targeted NPs has significantly promoted cell cycle arrest in the G1 phase by ~1.18 fold ($p < 0.01$) and ~1.32 fold ($P<0.001$), respectively, compared to the free PLB **(Figure 3.15).** The data obtained from the cell cycle analysis is in agreement with the MTT assay, cellular uptake, and apoptosis study.

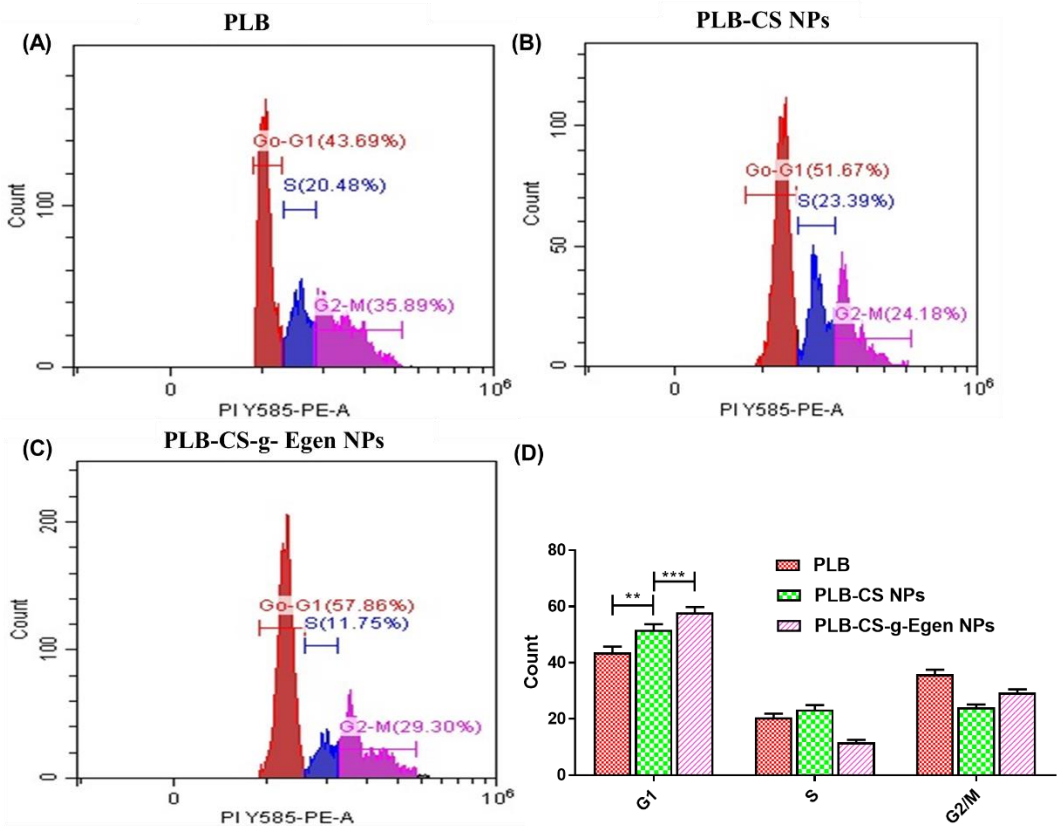

Figure 3.15 Cell cycle distribution analysis of MCF-7 cells after treatment with A) free PLB, B) PLB-CS NPs, and PLB-CS-g-Egen NPs. D) statistical comparison of cell cycle distribution analysis of Free PLB, PLB-CS NPs, and PLB-CS-g-Egen NPs.

3.5.5 Pharmacokinetic study

The pharmacokinetic profile and parameters of free PLB, PLB-CS NPs and PLB-CS-g-Egen NPs have been presented in **figure 3.16A** and **Table 3.4**. The graph showing PLB plasma concentration against the time after intravenous administration of 5.91 mg/kg equivalent dose of formulations. All the pharmacokinetic parameters were calculated by using Kinetica® 5.0. Entrapment of the PLB in the NPs has significantly improved the bioavailability of the PLB-CS NPs and PLB-CS-g-Egen NPs by 2.57 and 2.89-fold, respectively than PLB. Additionally, $T_{1/2}$ of the nontargeted and targeted NPs was increased by 1.90 and 1.93 fold compared to free PLB. Further, the AUCtotal of nontargeted NPs and targeted NPs was 2.57 and 2.89-fold higher, respectively, than that of free PLB. A nonsignificant difference in the pharmacokinetic parameter of nontargeted NPs and

targeted NPs was observed. Overall, incorporation of the PLB into the NPs has significantly improved the pharmacokinetic profile.

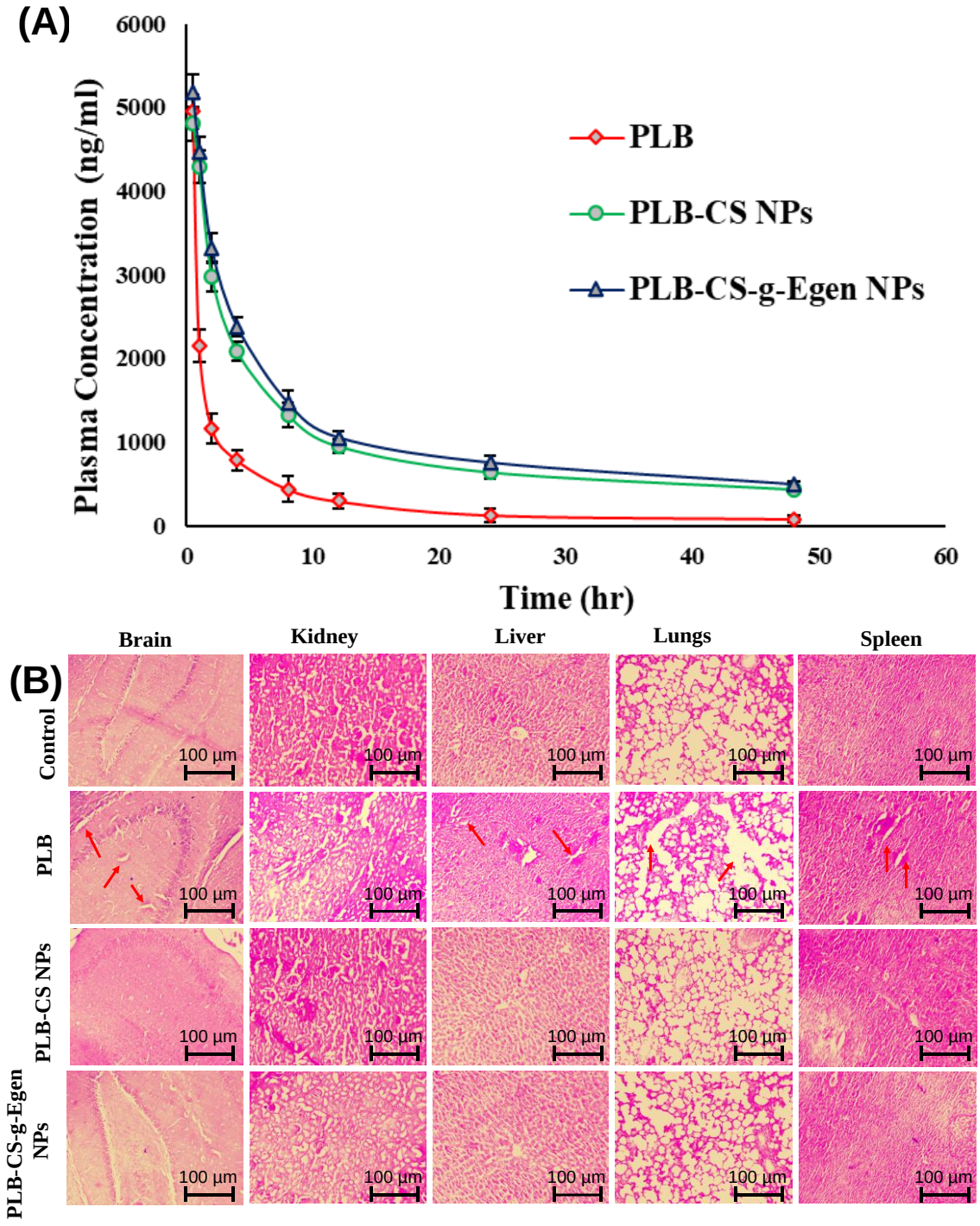

Figure 3.16 (A) Pharmacokinetic study showing plasma concentration vs time profile of drug concentration after intravenous administration of PLB, PLB-CS-g-Egen NPs and PLB-CS-g-Egen NPs, (B) Histopathological images of the rats vital organs after treatments with PLB. The arrow (red) indicates the location of the lesions.

Table 3.4 Pharmacokinetic parameters of PLB, non-targeted NPs (PLB-CS-g-Egen NPs) and targeted NPs (PLB-CS-g-Egen NPs) after i.v injection at an equivalent PLB dose of 5.91 mg/kg.

Parameters	**PLB (Mean ± SD*)**	**PLB-CS NPs (Mean ± SD*)**	**PLB-CS-g-Egen NPs (Mean ± SD*)**
AUC_{total} (ng.h/ml)	18382.37 ± 1265.76	47201.11 ± 1345.32	53196.62 ± 1264.62
C_{max} (ng/ml)	4948.94 ± 129.78	4808.03 ± 62.85	5186.33 ± 48.34
$T_{1/2}$ (h)	17.31 ± 0.62	32.90 ± 5.89	33.45 ± 6.05
MRT (h)	15.06 ± 0.35	39.16 ± 9.35	39.96 ± 4.87
V_d (l/kg)	1.45 ± 0.03	0.83 ± 0.04	0.74 ± 0.03
Cl_{total} (ml/kg.h)	57.92 ± 0.52	17.47 ± 0.95	15.39 ± 0.82
K_E (h^{-1})	0.040 ± 0.001	0.021 ± 0.004	0.020 ± 0.002
F_R	-	2.57	2.89

*n = 3; S.D: Standard deviation
Blank CS NPs: Blank chitosan nanoparticles
PLB-CS NPs: Non-targeted PLB loaded chitosan nanoparticles
PLB-CS-Egen NPs: Estrogen receptor targeted PLB loaded chitosan nanoparticles

3.5.6 Histopathology study

After administration of the free PLB, PLB-CS-g-Egen NPs and PLB-CS-g-Egen NPs at the dose of 5.914 mg/kg, vital organs (brain, lungs, liver, kidney, and spleen) harvested and processed for H & E staining. The different organ specimens were observed under a microscope and captured images were presented in **figure 3.16B**. The obtained histopathological images of the control rat were compared with NPs treated rats for identifying any toxicity associated with treatment with different formulations. Careful examination of the histopathological images of the control group of animals demonstrated that vital organs are free from pathological lesions. Animals receiving free PLB showed lesions in the brain, liver, lungs, and spleen. Nontargeted NPs have slightly improve the safety profile of the drug as demonstrated in the histopathological images. Finally, targeted NPs did not show any toxicity to the vital organs, and the images were similar to those of the control group of the animals [103].

3.5.7 *In vivo* antitumor activity by ultrasound/photoacoustic imaging

The breast tumor induced SD rats were subjected to photoacoustic and ultrasound imaging at 0 days (before treatments) and, 2nd day, 4th day, and 8th day of the post

treatments. The ultrasound/PA images of the breast tumor demonstrated a significant reduction of the breast tumor after the administration of the targeted NPs compared to the nontargeted and free PLB, whereas the tumor size was increased in the control animal receiving only saline (control group). On the 8th day, breast tumors completely vanished in the rats receiving targeted NPs (**Figure 3.17 A & B**).

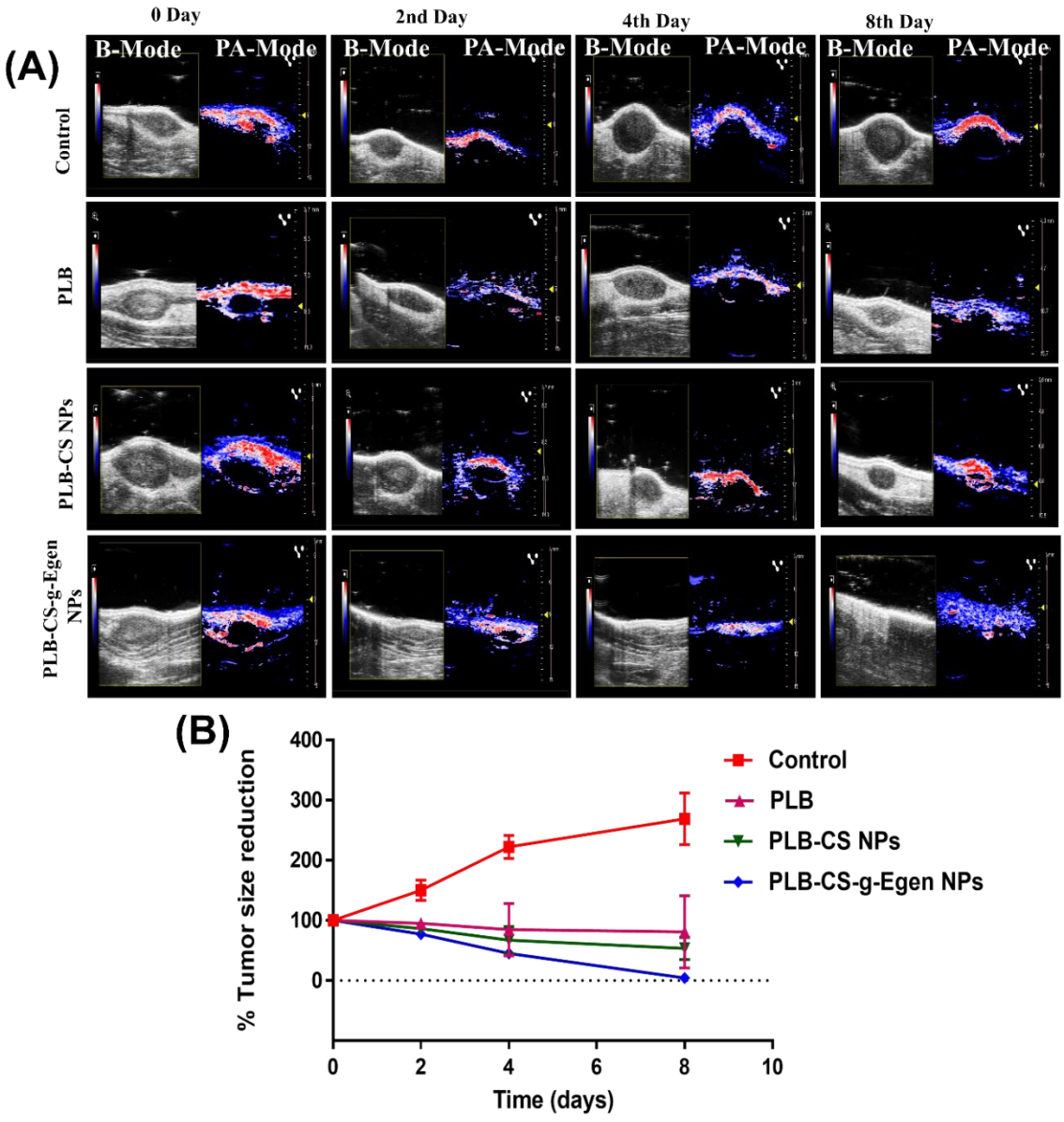

Figure 3.17 (A) Ultrasound and Photoacoustic imaging of the breast tumor before and after treatment with PLB, PLB-CS NPs, and PLB-CS-Egen NPs, (B) Effect of the treatments on the tumor size in rats with PLB, PLB-CS NPs and PLB-CS-Egen NPs.

Intratumoral hypoxia, which is primarily brought on by structural and functional anomalies in the vascular endothelium, is frequently linked to a more aggressive phenotype, a higher likelihood of metastasis, and therapeutic resistance [136]. Tumor with similar size and morphology may have different levels of hypoxia and tumor vascularity. At the beginning of the study, before the treatment, all group of the rats breast tumors was confirmed to have equivalent hypoxic tumor volume and tumor vascularity (**Figure 3.18**). After the treatments, the hypoxic tumor volume was significantly reduced in the NPs treatment group ($P< 0.05$), and at 8^{th} days after the treatments with targeted NPs, the hypoxic tumor volume completely vanished but the free PLB treated and nontargeted NPs treated group showed the hypoxic tumor volume of 24.18 ± 2.13 mm^3 and 17.45 ± 2.10 mm^3. Whereas in the case of the control group, hypoxic tumor volume (116.53 ± 5.11 mm^3) was significantly increased ($P< 0.0001$) relative to its 0 day hypoxic tumor volume (29.94 ± 1.02 mm^3) (**Figure 3.18 A & B**).

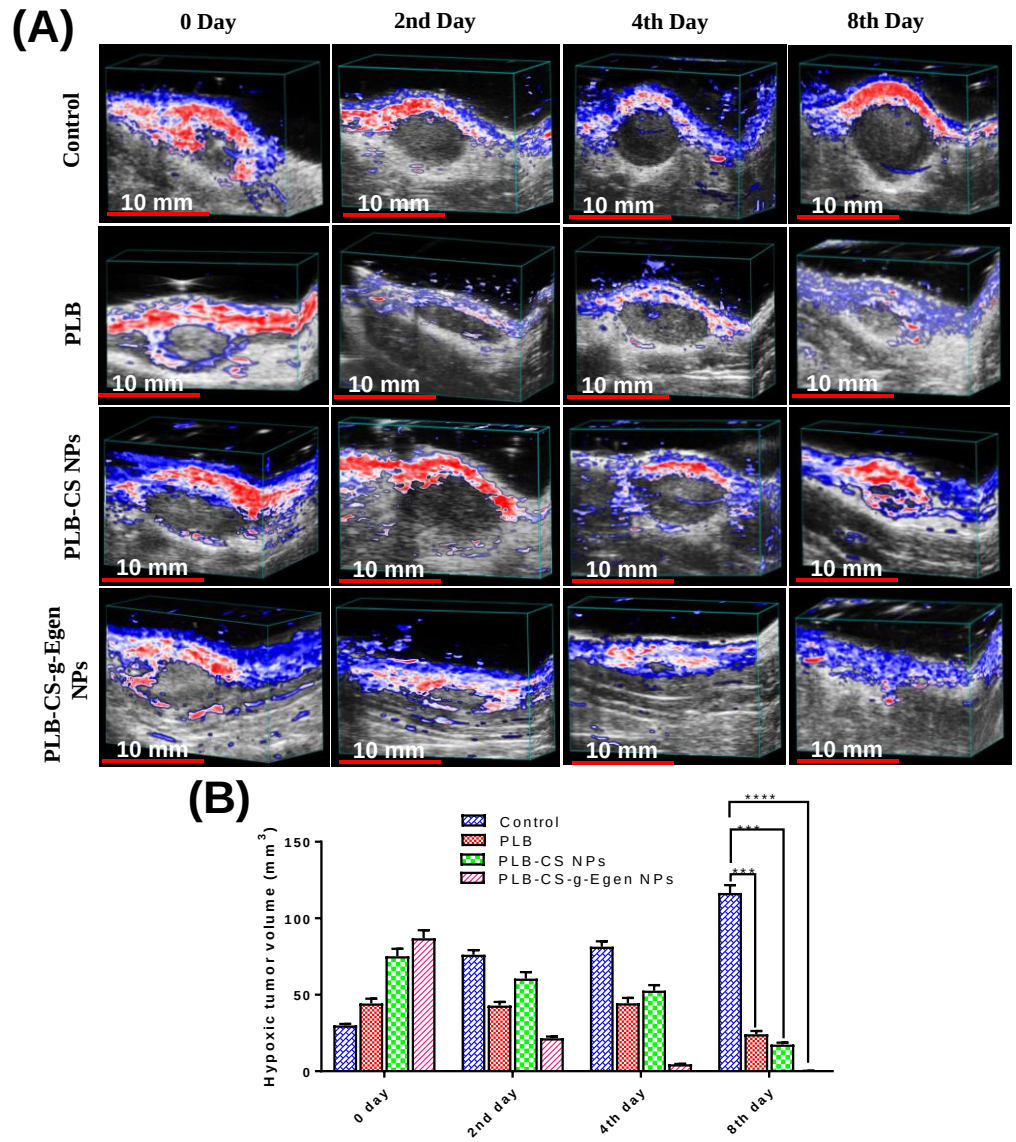

Figure 3.18 (A) Ultrasound and photoacoustic images of the breast tumor before and after treatment with PLB, PLB-CS NPs and PLB-CS-Egen NPs and (B) analysis of the hypoxic tumor volume.

For the proliferation of the tumor, it requires a continuous supply of the nutrients to the tumor cells in the higher amount that provoke the development of the blood vessels (angiogenesis) inside and outside of the tumor. After the treatment with targeted NPs, angiogenesis was stopped and further reduced as the days progressed and finally vanished at 8^{th} days of the treatments in the targeted treatments receiving animal group (**Figure 3.19 A & B**). Whereas the nontargeted NPs treatment group has a slight reduction in the tumor vasculature upto 4^{th} days but at the 8^{th} day after the treatments tumor vasculature was

significantly reduced. The free PLB treatment group also showed a slight reduction in tumor vasculature. Further, the control group of the rats shows increased tumor vasculature at 2nd days, slightly reduced at 4th days and further reduced at 8th days.

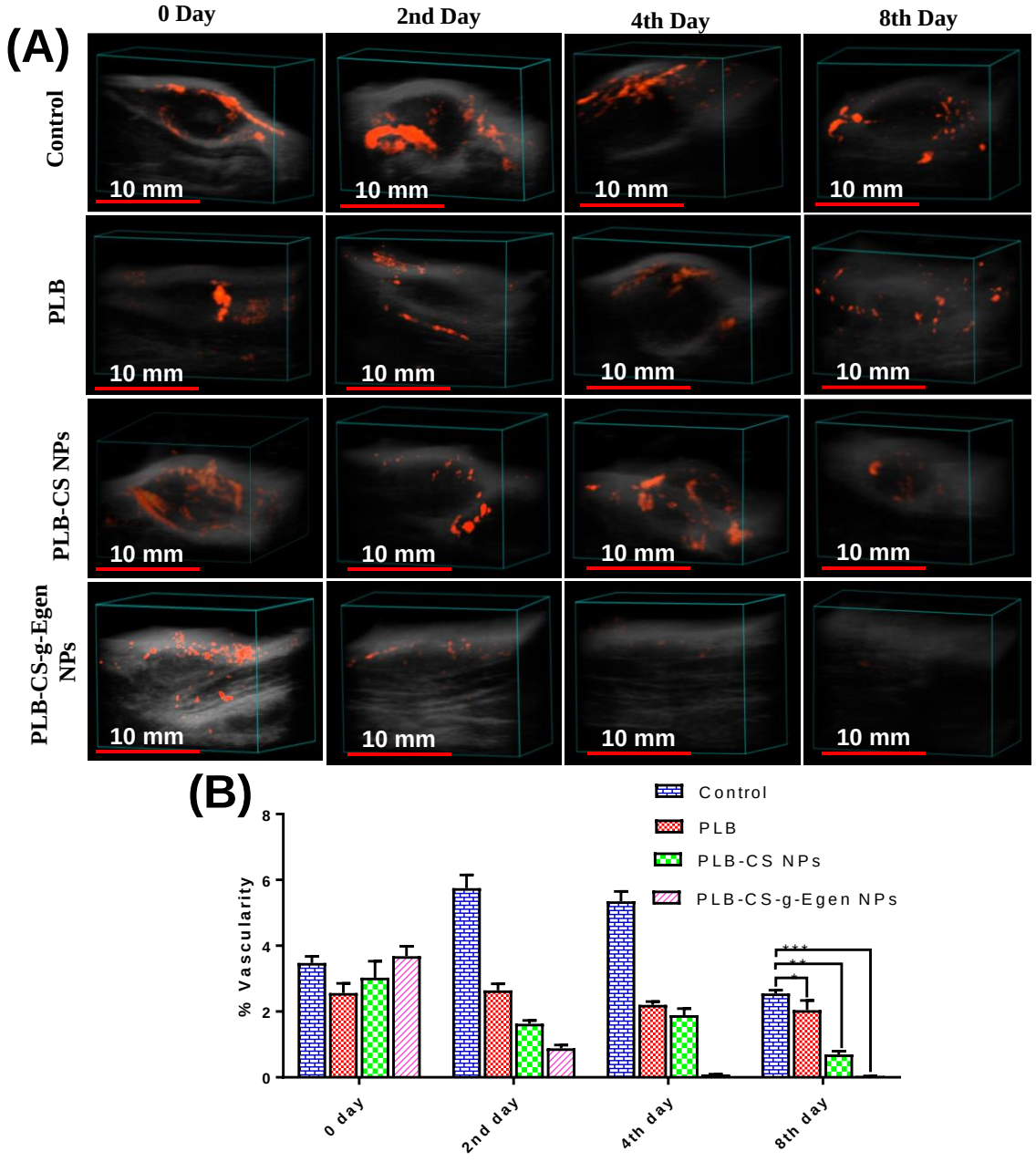

Figure 3.19 (A) Power Doppler images of the breast tumor before and after treatment with PLB, PLB-CS NPs and PLB-CS-Egen NPs and (B) analysis of angiogenesis and tumor vascularity.

Additionally, after the 8th days, these four groups of the rat's leftover tumor were extracted and subjected to H & E staining (**Figure 3.20**), and images were capturedd by using light microscope (400X).

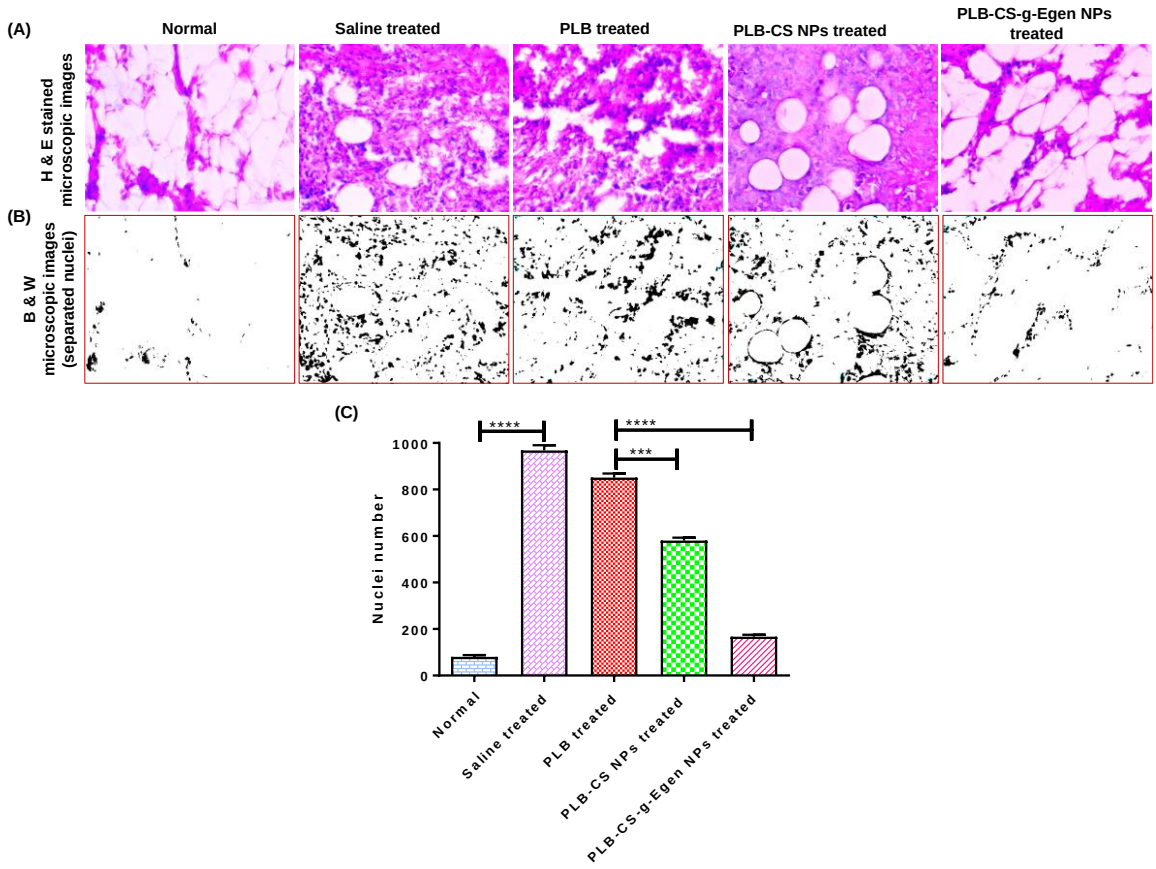

Figure 3.20 A) Histopathological H & E staining of normal, saline treated, PLB treated, PLB-CS NPs treated and PLB-CS-g-Egen NPs treated rat breast tumor sample. B) B&W images of separated nuclei of normal, saline treated, PLB treated, PLB-CS NPs treated and PLB-CS-g-Egen NPs treated rat breast tumor sample, C) histogram showing a number of separated nuclei from H & E and presented in B&W images.

The survival study in the DMBA induced breast tumor rats post-treatment is presented in **Figure 3.21**. The study was conducted for 18 weeks, and Kaplan−Meier survival analysis was performed to calculate the mean survival rate of the rats. The tumor bearing control rats receiving saline survived up to 5 weeks, whereas the PLB-treated rats survived up to 9 weeks. In rats treated with nontargeted NPs, 66.67% of the population survived up to 16 weeks, and the remaining rats were able to survive beyond 18 weeks. Rats treated with targeted NPs survived beyond 18 weeks, and their survival was similar to that of healthy rats.

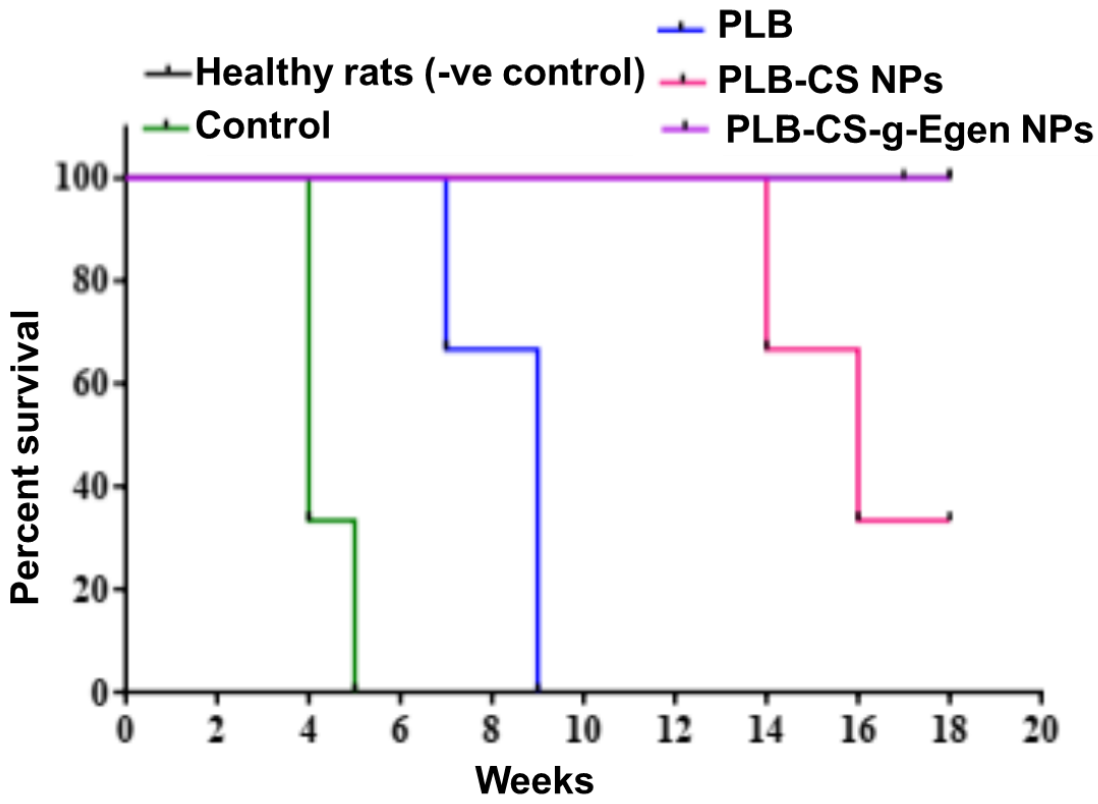

Figure 3.21. Kaplan-Meier survival analysis plot. Healthy rats and PLB- CS-g-Egen NPs treated rats had 100 % survival (back and violet lines superimposed).

3.5.8 *In vivo* breast tumor targeting efficiency by IVIS live imaging

In vivo, fluorescence imaging (**Figure 3.22**) demonstrated that free DiD (control), DiD-CS NPs, and DiD-CS-g-Egen NPs were distributed to different body parts within 2 h. After 2 h of the administration, targeted NPs started accumulating in the breast tumor, but free DiD and nontargeted NP fluorescent signals were significantly less at the site of the tumor. Further, after 6 h of administration, it was observed that targeted NPs completely accumulated to the tumor site, whereas free DiD and nontargeted NP signals were still less at the tumor site. Moreover, after 8 h, the concentration of the targeted NPs started declining at the tumor site, which may be due to the metabolism or degradation of the NPs in the tumor microenvironment. Additionally, the image (**Figure 3.22B**) of the control rat (without DiD administration) does not show any fluorescent or background signal. The quantitative radiant efficiency signal from the free DiD, DiD-CS NPs, and DiD-CS-g-Egen

NPs after administration is presented in **Figure 3.22C.** These results confirm the targeted delivery of CS-g-Egen NPs to breast tumors.

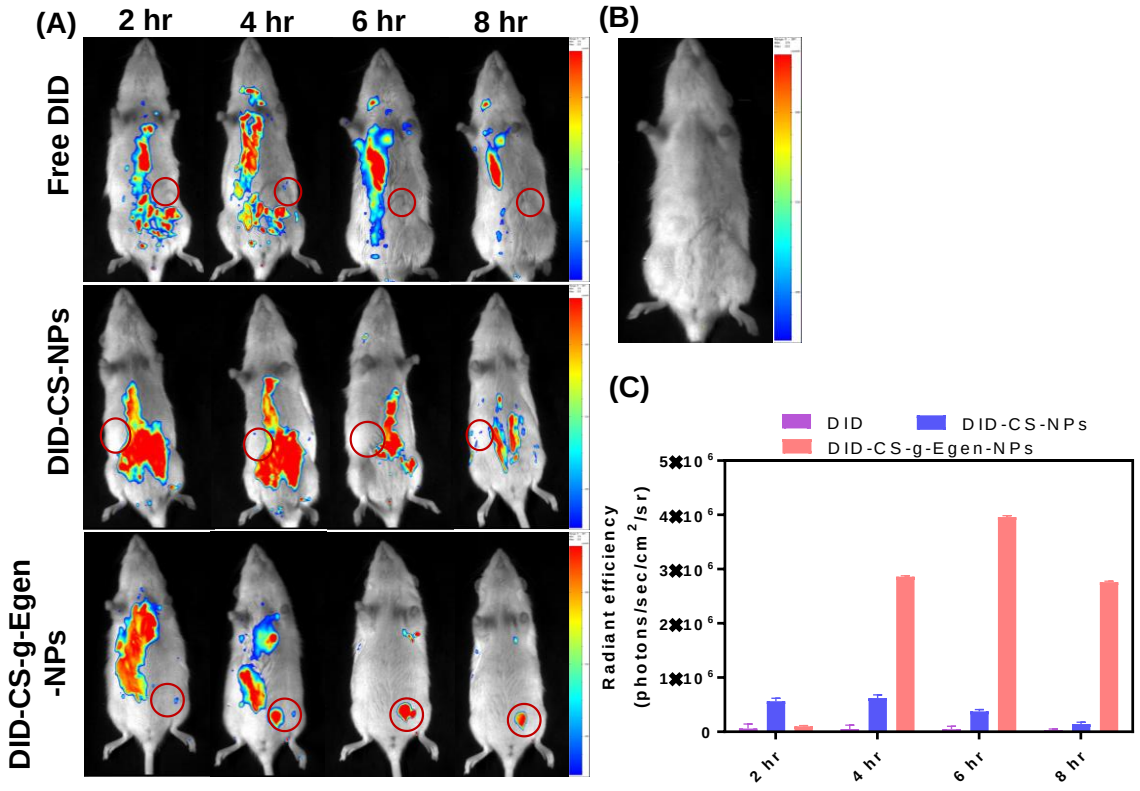

Figure 3.22. A) *In vivo* biodistribution in DMBA induced breast cancer model, and (B) Control rat imaging without DiD administration. C) Histogram showing radiant efficiency at different time intervals.

3.6 Conclusion

In this research work, an Egen functionalized CS-based graft polymeric nano drug delivery system was developed for the targeted delivery of PLB to the ER-positive breast tumor. The entrapment efficiency of the PLB in the NPs was found to be up to 75.79%, which confirms that solvent evaporation followed by the ionic gelation method was suitable for the preparation of the NPs. The DLS, FE-SEM, TEM, and AFM analyses demonstrated that NPs were spherical in shape and had smooth surfaces. The presence of Egen on the outer surface of targeted NPs was confirmed by XPS analysis. The *in vitro* drug release study depicted that NPs were found to have sustained drug-releasing properties. The developed targeted NPs had more apoptosis-inducing properties compared with

nontargeted NPs and free PLB, which were confirmed by the apoptosis study and cell cycle analysis. Targeted NPs were efficiently accumulated into the MCF-7 cells and T-47D cells as demonstrated in the cellular uptake study, and pretreatment of the cells with free Egen reduced the cellular uptake of the targeted NPs due to ER saturation, which confirms the receptor mediated endocytosis of the targeted NPs. The *in vitro* cytotoxicity assay in MCF-7 cells and T-47D cells suggested that targeted NPs were 57.34- and 30.32-fold more cytotoxic than the pure PLB, respectively. There was a 2−3-fold enhancement in the half-life and bioavailability of the NPs due to the entrapment of the PLB inside the NPs. The targeted NPs were capable of vanishing the DMBA induced breast tumor within 8 days of treatment, which was confirmed by ultrasound and photoacoustic imaging. Additionally, targeted NPs were capable of reducing the hypoxic tumor volume and tumor vascularity more efficiently compared with nontargeted and free PLB. Additionally, the biocompatibility and safety of the NPs were confirmed by an *in vitro* hemocompatibility and histopathology study. In summary, the developed targeted NPs showed great potential for delivering PLB to ERs-expressing hypoxic breast tumors.